Journal of Colloid and Interface Science 368 (2012) 342–355

Contents lists available at SciVerse ScienceDirect

Journal of Colloid and Interface Science

www.elsevier.com/locate/jcis

Role of surfactants on the approaching velocity of two small emulsion drops

Krassimir D. Danov [a], Simeon D. Stoyanov [b,c,*], Nikolay K. Vitanov [d], Ivan B. Ivanov [e]

[a] Department of Chemical Engineering, Faculty of Chemistry, Sofia University, Sofia 1164, Bulgaria
[b] Unilever Research & Development, 3133 AT Vlaardingen, The Netherlands
[c] Laboratory of Physical Chemistry and Colloid Science, Wageningen University, 6703 HB Wageningen, The Netherlands
[d] Laboratory of Physicochemical Hydrodynamics, Institute of Mechanics, Bulgarian Academy of Science, Sofia 1113, Bulgaria
[e] Laboratory of Chemical Physics and Engineering, Faculty of Chemistry, Sofia University, Sofia 1164, Bulgaria

ARTICLE INFO

Article history:
Received 12 August 2011
Accepted 12 November 2011
Available online 25 November 2011

Keywords:
Hydrodynamic resistance between two approaching drops
Tangentially mobile surfaces
Soluble and insoluble surfactants
Interfacial rheology effect
Flocculation rate of emulsion droplets
Small Reynolds and Peclet numbers

ABSTRACT

Here we present the exact solution of two approaching spherical droplets problem, at small Reynolds and Peclet numbers, taking into account surface shear and dilatational viscosities, Gibbs elasticity, surface and bulk diffusivities due to the presence of surfactant in both disperse and continuous phases. For large interparticle distances, the drag force coefficient, f, increases only about 50% from fully mobile to tangentially immobile interfaces, while at small distances, f can differ several orders of magnitude. There is significant influence of the degree of surface coverage, θ, on hydrodynamic resistance β for insoluble surfactant monolayers. When the surfactant is soluble only in the continuous phase the bulk diffusion suppresses the Marangoni effect only for very low values of θ, while in reverse situation, the bulk diffusion from the drop phase is more efficient and the hydrodynamic resistance is lower. Surfactants with low value of the critical micelle concentration (CMC) make the interfaces tangentially immobile, while large CMC surfactants cannot suppress interfacial mobility, which lowers the hydrodynamic resistance between drops. For micron-sized droplets the interfacial viscosities practically block the surface mobility and they approach each other as solid spheres with high values of the drag coefficient.

1. Introduction

The stability of emulsions (foams) under dynamic conditions depends on the hydrodynamic resistance between drops (bubbles), β, on the non-hydrodynamic interactions energy, $U_{i,j}$, between their interfaces, and interparticle distance, h [1–5]. In the general Smoluchowski scheme for flocculation, the flocculation rates, $a_{i,j}$, between two spherical colloid particles with radii R_i and R_j can be calculated from the expression [1,3,6–9]:

$$a_{i,j} = 8\pi k_B T \left[\int_{h_{cr}}^{\infty} \frac{\beta(h)}{(h + R_i + R_j)^2} \exp\left(\frac{U_{i,j}}{k_B T}\right) dh \right]^{-1}, \tag{1.1}$$

where k_B is the Boltzmann constant and T is the temperature. For given force $F(h)$ acting on the colloidal particles and approaching velocity $V(h)$, the hydrodynamic resistance is defined as follows:

$$\beta(h) \equiv \frac{F(h)}{V(h)}. \tag{1.2}$$

The integral in Eq. (1.1) is taken over the interparticle separation, h, starting from the critical thickness, h_{cr}. For unstable films h_{cr} represents the distance at which the film between drops (bubbles) breaks. Droplets flocculate, when the film formed upon their collision is stable, with h_{cr}, being equilibrium film thickness distance. The integral in Eq. (1.1) is proportional to the so-called Fuchs factor [1,10] and its reciprocal value defines the collision efficiency [3,11,12]. For larger values of the Fuchs factor (smaller values of the collision efficiency) the flocculation rates are smaller and the emulsions (foams) are more stable under dynamic conditions.

Except of the energy of non-hydrodynamic interactions, $a_{i,j}$ depends considerably on the hydrodynamic resistance. For large interparticle distances β is a constant, while for small h, the hydrodynamic friction in the gap between particles increases orders of magnitude, which makes the precise hydrodynamic calculations of β of a fundamental importance. Stimson and Jeffery [13] solved the axisymmetric problem of two solid spheres translating at an equal velocity along their line of centers. Cooley and O'Neill [14] recalculated their results for the more general case when the two spheres are not of equal size. For small gap widths G.I. Taylor showed that $\beta \propto 1/h$, whose result is widely used in the literature [1] (in fact the Taylor solution does not appear in any G.I. Taylor's publications but in the article by Hardy and Bircumshaw [15] it was published [16]).

The exact solution of the problem for the motion of two liquid droplets along their line of centers in a quiescent fluid is reported in bispherical coordinates in Refs. [17–19]. Davis et al. [20,21] found asymptotic and numerical results for the hydrodynamic

* Corresponding author at: Unilever Research & Development, 3133 AT Vlaardingen, The Netherlands. Fax: +31 10 460 6384.
E-mail address: simeon.stoyanov@unilever.com (S.D. Stoyanov).

0021-9797/$ - see front matter Crown Copyright © 2011 Published by Elsevier Inc. All rights reserved.
doi:10.1016/j.jcis.2011.11.031

lubrication resistance force correspondent to different drops viscosities and gap widths. For small interparticle distances the hydrodynamic resistance has different asymptotic depending on the viscosity of disperse phase [20–26]: in the case of bubbles $\beta \propto \ln(h)$; in the case of droplets $\beta \propto h^{-1/2}$. For large distances the values of β correspond to the Hadamard–Rybczynski drag force. Thus, the ratio between the drop and continuous phase viscosities, that is the mobility of interface, is of a major importance for the magnitude of the hydrodynamic friction force, especially at small gap widths between the colloidal particles.

The surface active species (ionic and nonionic surfactants, proteins, polymers, etc.) are used to stabilize all real emulsions and foams. The surfactants adsorb on the interfaces, decrease the interfacial tension, and affect the dynamic behavior of colloidal systems as follows. First, the surfactant adsorption modifies the nonhydrodynamic interactions between surfaces at small gap widths. This effect is accounted for including the different components of the disjoining pressure (van der Waals attraction, electrostatic and steric repulsion, hydrophobic and structural interactions, etc.) into the interaction force between colloidal particles, see Eq. (1.1) and Refs. [27,28]. Second, the surfactants increase the hydrodynamic resistance and modify the interfacial rheology of drops and bubbles [3–5,29–31]. Non-uniform adsorption creates nonuniform interfacial tension forces and Marangoni stresses in the fluid. The bulk and surface diffusions tend to restore the uniform surfactant distribution and suppress the Marangoni effect. The interfacial shear and dilatational viscosities play important role for lowering the interfacial mobility – this is the major effect for micron-sized colloidal particles, which leads to tangentially immobile interfaces for all interparticle distances.

Most studies of the hydrodynamic problem for approaching of drops and bubbles for small and arbitrary values of the Peclet number consider the effect of insoluble surfactants [32–35]. The role of bulk diffusion in the case of soluble surfactants is described in the recent works, see Refs. [36,37]. In all publications [32–37]: (i) the interfacial viscosities do not taken into account; (ii) the numerical calculations are very complex; (iii) they account also for the deformation of colloidal particles, describe the general phenomena, but are so time consumable that the incorporation of these computations in Eq. (1.1) for the prediction of the dependence of flocculation rates on the physicochemical parameters is rather difficult. The mutual approach and stability of two bubbles in lubrication approximation is studied in Refs. [38,39]. The material properties of the interfaces (surface viscosities, Gibbs elasticity, surface and bulk diffusivity) are taken into account and some asymptotic formulae are reported [38,39]. Nevertheless, the precise calculations of the Fuchs factor, see Eq. (1.1), need the knowledge of the hydrodynamic resistance for all interparticle distances and the use only of the asymptotic expressions may lead to wrong conclusions.

If the applied force between the colloid particles is large enough, then the drops (bubbles) deform and an almost plane-parallel film between them is formed. In this case the role of surfactants on the hydrodynamic friction force can be studied only numerically because of the complex geometry of colloid particles. In the asymptotic case of lubrication approximation the problem is considered in Refs. [40–45]. The authors have shown that the solubility of surfactants in the continuous phase plays important role for suppressing the Marangoni effect and the film drainage is accelerated with respect to the case when the surfactants are soluble only in the continuous phase.

Here, our goal is to directly calculate the hydrodynamic resistance of two approaching spherical drops (bubbles) for small Reynolds numbers in the presence of surfactants soluble in disperse and/or continuous phase. The deformability of the colloidal particles is not taken into account because of the numerical difficulties of the respective problem. The role of interfacial rheology, Marangoni effect, bulk and surface diffusivities is accounted for in the model equations (Section 2). For small deviation of adsorption from its equilibrium value the exact solution of the problem in bipolar coordinates is described (Sections 3 and 4). Some useful asymptotic solutions are reported and the numerical results for different systems are discussed in Section 5.

2. Physical system and basic equations

We consider two identical drops (bubbles) approaching each other with a given velocity, V (Fig. 1). The physicochemical parameters of the fluid phase inside the drops (the disperse phase) will be denoted with the subscript "d", while the respective parameters of the continuous fluid phase – with the subscript "f". For example, the mass densities are denoted as ρ_d and ρ_f, the dynamic viscosities – as η_d and η_f, the vectors of the fluid velocity are $\mathbf{v}_d$ and $\mathbf{v}_f$, and the pressures in the respective phases are p_d and p_f. We are interested in the hydrodynamic interactions between small bubbles and drops when the distances between them and the relative fluid velocity are small. In these cases the Reynolds numbers are so small that the flow can be considered as a viscous, incompressible creeping motion, which obeys the Stokes equations [2,29]:

$$\nabla \cdot \mathbf{v}_k = 0, \quad \nabla p_k = \eta_k \nabla^2 \mathbf{v}_k \ (k = \mathrm{f}, \mathrm{d}), \tag{2.1}$$

where ∇ is the gradient operator and ∇^2 is the Laplace operator.

Generally, both phases can contain dissolved surface-active components (ionic and nonionic surfactants, protein isolates, etc.) used for stabilization of emulsions and foams. We will assume that the bulk solutions in the respective phases contain one type of surface-active component with concentrations c_d and c_f, which are below the critical micelle concentrations (CMC). The bulk diffusion equations read [29,46]

$$\frac{\partial c_k}{\partial t} + \nabla \cdot (c_k \mathbf{v}_k) = D_k \nabla^2 c_k \ (k = \mathrm{f}, \mathrm{d}), \tag{2.2}$$

where t is time and D_f and D_d are the bulk diffusion coefficients in the continuous and disperse phases, respectively.

To account for the influence of surfactants, we consider the Boussinesq–Scriven constitutive law for the interfaces [47,48]. Then the Newtonian surface-excess stress tensor, $\mathbf{S}$, can be defined in the following form [29]

$$\mathbf{S} = \sigma \mathbf{I}_s + (\eta_{dil} - \eta_{sh})(\mathbf{I}_s : \mathbf{D}_s)\mathbf{I}_s + 2\eta_{sh}\mathbf{D}_s, \tag{2.3}$$

where $\mathbf{I}_s$ is the unit surface idemfactor, $\mathbf{D}_s$ is the rate of relative displacement of surface points, σ is the interfacial tension, η_{dil} and η_{sh} are the surface dilatational and shear viscosities at a given point of the interface, respectively. It is important to note that Eq. (2.3) includes the surface dilatational and shear viscosities. In rheological experiments with oscillations of drops or bubbles the elastic and loss modules are measured [49]. The value of the loss modulus, E'', multiplied by the frequency, ω, is usually called "the surface viscosity", which has different meaning than η_{dil} and η_{sh} [31]. The true

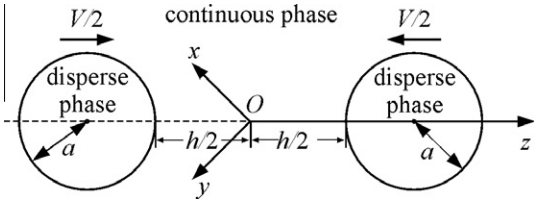

Fig. 1. Sketch of two spherical drops with equal radii, a, which stay at a closest distance between them, h. The drops move toward each other with given approaching velocity V. The z-axis of Cartesian coordinate system $Oxyz$ coincides with the axis of revolution and the plane $z = 0$ represents the plane of symmetry of the system.

surface shear and dilatational viscosities, η_{dil} and η_{sh}, are measured using different experimental techniques [29] and have the same dimensions as the apparent viscosity, $\omega E''$, but considerably different values [50–52].

The tensor $\mathbf{D}_s$ constitutes the symmetric portion of the dyadic of the surface-velocity vector $\mathbf{v}_s$ [29], i.e.

$$2\mathbf{D}_s \equiv (\nabla_s \mathbf{v}_s)\cdot\mathbf{I}_s + \mathbf{I}_s\cdot(\nabla_s \mathbf{v}_s)^{tr}, \tag{2.4}$$

where ∇_s is the surface gradient operator and the superscript "tr" means transposition. Eqs. (2.3) and (2.4) are the two dimensional analogs to the comparable expressions for the bulk phase pressure tensor $\mathbf{P}_k$ and the three-dimensional rate of deformation tensor $\mathbf{D}_k$, respectively, and

$$\mathbf{P}_k = -p_k\mathbf{I} + 2\eta_k\mathbf{D}_k \quad (k = \mathrm{f},\mathrm{d}), \tag{2.5}$$

$$2\mathbf{D}_k \equiv (\nabla\mathbf{v}_k)\cdot\mathbf{I} + \mathbf{I}\cdot(\nabla\mathbf{v}_k)^{tr} \ (k = \mathrm{f},\mathrm{d}). \tag{2.6}$$

Because in all practical circumstances the surface-excess mass density is small compared to the bulk-phase mass density the equation for the interfacial momentum transport is simplified to the surface stress boundary condition. In our case we have [29,48]

$$\nabla_s\cdot\mathbf{S} = \mathbf{n}_s\cdot(\mathbf{P}_d - \mathbf{P}_f), \tag{2.7}$$

written at the mathematical surface between phases with outer unit normal vector $\mathbf{n}_s$.

For concentrations above the critical micelle concentrations the relaxation time of surfactants is very low (in the order of microseconds [53,54]) and the change of adsorption can be neglected. In this case the Marangoni effect, which is described by the $\nabla_s\sigma$ in the left-hand side of Eq. (2.7), is negligible compared to the Boussinesq–Scriven effect, accounting for the surface viscosity (see Section 5.2).

To close the boundary problem, Eqs. (2.1)–(2.7), the mass balance equation for the adsorption Γ at the interface is included in the considerations [29]:

$$\frac{\partial\Gamma}{\partial t} + \nabla_s\cdot(\mathbf{v}_s\Gamma - D_s\nabla_s\Gamma) = \mathbf{n}_s\cdot(D_f\nabla c_f - D_d\nabla c_d). \tag{2.8}$$

Eq. (2.8) says that the change of adsorption is balanced by the bulk diffusion fluxes from the contiguous bulk phases, the surface convection flux, and the surface diffusion flux with surface diffusivity D_s.

The adsorption processes can be classified as diffusion controlled and barrier controlled. As a rule the barrier control of the adsorption is operative at the initial stages, when the whole process cannot be considered as a steady state thinning of the film between droplets (these are the cases of intensive emulsification and foaming in turbulent regimes) [55]. In the case of slow laminar flows the diffusion control is dominant and the adsorption mechanism is diffusion controlled. During the whole film drainage in this regime, the adsorption and interfacial tension are related to the subsurface concentrations with the respective isotherm and two-dimensional equation of state [3,29]. Moreover, for small values of the Peclet number (small drainage velocities and radii) the deviations of the concentrations and adsorption, c_f, c_d, and Γ, from their respective values at rest (when $V = 0$), $c_{f,0}$, $c_{d,0}$, and Γ_0, are small. These deviations are denoted as

$$\Gamma \equiv \Gamma_0 + \Gamma_1, \quad c_k \equiv c_{k,0} + c_{k,1} \ (k = \mathrm{f},\mathrm{d}). \tag{2.9}$$

The assumption (2.9) makes possible: (i) to reduce the bulk diffusion equations to the Laplace equation for the concentrations

$$\nabla^2 c_{k,1} = 0 \ (k = f, d); \tag{2.10}$$

(ii) to simplify the condition for the mass balance of surfactants at the interface, Eq. (2.8), to its linear form

$$\nabla_s\cdot(\mathbf{v}_s\Gamma_0 - D_s\nabla_s\Gamma_1) = \mathbf{n}_s\cdot(D_f\nabla c_{f,1} - D_d\nabla c_{d,1}); \tag{2.11}$$

(iii) to express the subsurface concentrations, $c_{k,s}$, as linear functions of the deviation of adsorption at the interface

$$c_{k,s} = c_{k,0} + \left(\frac{\partial c_k}{\partial\Gamma}\right)_0\Gamma_1 \ (k = \mathrm{f},\mathrm{d}); \tag{2.12}$$

(iv) to transform the two-dimensional equation of state, $\sigma = \sigma(\Gamma)$, in its linear form

$$\sigma = \sigma(\Gamma_0) - E_G\frac{\Gamma_1}{\Gamma_0}, \tag{2.13}$$

where E_G is the Gibbs elasticity of the interface corresponding to the adsorption at rest, which is defined as [3,29]

$$E_G \equiv -\left(\frac{\partial\sigma}{\partial\ln\Gamma}\right)_0. \tag{2.14}$$

The derivatives appearing in the right-hand side of Eq. (2.12) represent the reciprocal values of the respective adsorption lengths. Note that $(\partial c_k/\partial\Gamma)_0$ and E_G can vary several orders of magnitude depending on the concrete physicochemical parameters (see Section 5.1).

The two critical limitations of the linearized problem are that the Peclet number, Pe, has to be small, and that the droplets should not deform as they approach each other. At large interparticle distances, Pe is defined as Va/D_k. If the buoyancy force is essential, then Pe is proportional to the density difference and a^3. In the case of gas-in-water dispersions, the assumption of low Peclet number is fulfilled for micron-sized bubbles. For emulsions, the density difference is small, so that Pe can be small even for larger drops. Note, that for small interparticle distances, the Peclet number is rescaled with $\sinh\varepsilon$ (see Section 3), that is the Peclet number decreases and the applicability of the linear model becomes wider. The capillary number, $\sigma/(\eta_k V)$, characterizes the droplet deformability. For large capillary numbers, the droplets preserve their spherical form. In the case of buoyancy force, the velocity, V, is proportional to a^2 and then bubbles larger than 5 mm deform. Moreover, the capillary number becomes $\propto\sigma/(\eta_k a^2)$. The interfacial tension of emulsion drops is considerably lower than that of bubbles, but the typical dimensions of the drops are much smaller than of the bubbles, so that in a final reckoning, the capillary number in emulsions is larger than that in foams.

3. Exact solution of the Stokes equations in bipolar coordinates

3.1. General solution of the Stokes equations

For small particle sizes, a, the capillary numbers are small and the possible deformations of the interfaces can be neglected when the leading order solution of the problem is derived. Thus, the considered problem is steady state, the drainage velocity is $V = -dh/dt$, and the analytical solution of the simplified problem for non-deformed droplets (bubbles) can be obtained in bipolar coordinates. First, one introduces Cartesian coordinate system $Oxyz$, in which the z-axis coincides with the axis of revolution and plane $z = 0$ represents the plane of symmetry of the system (Fig. 1). The respective cylindrical coordinate system has radial coordinate r, polar angle φ, and

$$x = r\cos\varphi, \quad y = r\sin\varphi. \tag{3.1}$$

The bipolar coordinates, x_1 and x_2, are defined with respect to the positions of the poles at the axis of revolution with coordinates $z = \pm c$ (see Fig. 2) as [18,19]

$$r = \frac{c}{b}\sin x_2, \quad z = \frac{c}{b}\sinh x_1, \tag{3.2}$$

$$b \equiv \cosh x_1 - \cos x_2. \tag{3.3}$$

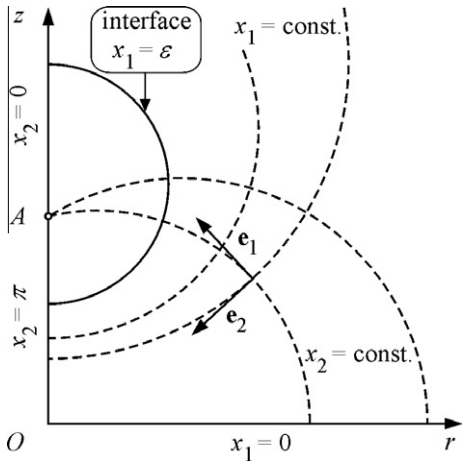

Fig. 2. Introduction of bipolar coordinates (x_1, x_2). The cylindrical coordinates are (r, φ, z) (see Fig. 1), the plane of symmetry is $x_1 = 0$, the pole A corresponds to $x_1 \to +\infty$, and the position of the drop surface coincides with coordinate surface $x_1 = \varepsilon$.

The plane of symmetry ($z = 0$) corresponds to $x_1 = 0$ in these coordinates. The part of the axis of revolution, for which $|z| > c$, is described by $x_2 = \pi$, while that, for which $|z| < c$ – by $x_2 = 0$ (Fig. 2). The positions of both poles are obtained as limiting values for $x_1 \to \pm\infty$.

Coordinate surfaces $x_1 = \text{const.}$ are spheres with radius $|c/\sinh x_1|$ and center $z = c/\tanh x_1$ at the axis of revolution (Fig. 2). Therefore, if the droplet surfaces are defined with coordinates $x_1 = \pm\varepsilon$, then the values of ε and coordinate c of pole A (Fig. 2) are determined from the relationships

$$\cosh\varepsilon = 1 + \frac{h}{2a}, \quad c = a\sinh\varepsilon. \tag{3.4}$$

In bipolar coordinates the region occupied by the continuous phase is given by $|x_1| < \varepsilon$, while that corresponding to the droplet phase – by $|x_1| > \varepsilon$. For small film thicknesses ($h \ll a$) we have $\varepsilon \approx (h/a)^{1/2}$ and $c \approx (ah)^{1/2}$.

Because of the linearity of the Stokes equations we can invert the flow [18,19], i.e. we will assume that the droplet above the plane of symmetry is at rest and the velocity in the plane of symmetry obeys the conditions

$$v_{f,1} = \frac{V}{2}, \quad \frac{\partial v_{f,2}}{\partial x_1} = -\frac{V}{2}\cot\left(\frac{x_2}{2}\right) \text{ at } x_1 = 0. \tag{3.5}$$

For this flow the normal component of the fluid velocity at the drop surface is zero ($v_{f,1} = v_{d,1} = 0$ at $x_1 = \varepsilon$) and the tangential components of the velocities are equal to the surface velocity component u, i.e. $v_{f,2} = v_{d,2} = u$ at $x_1 = \varepsilon$.

The stream function, ψ_k, for any axisymmetric Stokes' flow is well known to satisfy the general equations [18,19]

$$v_{k,1} = \frac{b^2}{c^2\sin x_2}\frac{\partial\psi_k}{\partial x_2}, \quad v_{k,2} = -\frac{b^2}{c^2\sin x_2}\frac{\partial\psi_k}{\partial x_1} \ (k = \mathrm{f}, \mathrm{d}) \tag{3.6}$$

$$E^2 \equiv r\frac{\partial}{\partial r}\left(\frac{1}{r}\frac{\partial}{\partial r}\right) + \frac{\partial^2}{\partial z^2} \text{ and } E^4(\psi_k) = 0 \ (k = \mathrm{f}, \mathrm{d}). \tag{3.7}$$

Stimson and Jeffery's general solution of Eq. (3.7) may be expressed in the following form [13]

$$\psi_k = b^{-3/2}\sum_{n=1}^{\infty} U_{k,n}(x_1)V_n(\xi) \ (k = \mathrm{f}, \mathrm{d}), \tag{3.8}$$

where $\xi \equiv \cos x_2$; $V_n = P_{n+1} - P_{n-1}$; P_n is the Legendre polynomial [56]; the functions $U_{k,n}(x_1)$ are simple linear superposition of the four exponential functions, $\exp(\lambda_{n-1}x_1)$, $\exp(\lambda_{n+1}x_1)$, $\exp(-\lambda_{n-1}x_1)$, and $\exp(-\lambda_{n+1}x_1)$; the parameter λ_n is defined as

$$\lambda_n \equiv n + \frac{1}{2}. \tag{3.9}$$

If the surface velocity is known, that is the coefficients, u_n, of the serial expansion

$$u = \frac{(2b)^{1/2}V}{2\sin x_2\sinh\varepsilon}\sinh\left(\frac{\varepsilon}{2}\right)\sum_{n=1}^{\infty} n(n+1)\frac{u_n}{\lambda_n}V_n(\xi) \tag{3.10}$$

of function $u(x_2)$ describing the tangential component of the surface velocity are known, then the solution for the stream functions, ψ_d and ψ_f, is given by Eqs. (A.1)–(A.7), see Appendix A and Refs. [18,57].

3.2. Hydrodynamic drag force

From a physical viewpoint it is important to calculate the hydrodynamic drag force acting on the droplet (bubble). Because of the symmetry the drag force, F, has only z component, which is directed oppositely to the velocity of the respective drop. The characteristic of the magnitude of this force is the drag force coefficient, f, defined as

$$F \equiv \pi\eta_f a V f. \tag{3.11}$$

Substituting solution Eq. (A.2) into the general series for the hydrodynamic drag force from Ref. [18] we obtain that

$$f = f_{im} - 8\sinh\varepsilon\sinh\left(\frac{\varepsilon}{2}\right)\sum_{n=1}^{\infty} n(n+1)\cosh(\lambda_n\varepsilon)\frac{u_n}{\Delta_n}, \tag{3.12}$$

where f_{im} is the drag force coefficient corresponding to the case of *tangentially immobile interfaces* and coefficients Δ_n are calculated from Eq. (A.3).

Stimson and Jeffery's formula [13,57] for the drag force coefficient, f_{im}, in the case of solid spheres approaching each other with a given velocity, V, is reported in Appendix A, Eq. (A.8). Eq. (A.8) has a simple asymptotic form for small interparticle distances, Eq. (A.9), known as Taylor's formula. The comparison of the calculated results by means of Eq. (A.8) and Eq. (A.9) is illustrated in Fig. 3. Eq. (A.10) represents the asymptotic expression for f_{im} valid at large interparticle distances. For $a/h \to 0$ the value of $f_{im} \to 3$ because the velocity of the individual particle is $V/2$ and the Stokes formula reads $F = 6\pi\eta_f a(V/2) = 3\pi\eta_f aV$. It is important to note that all asymptotic series, like Eq. (A.10), converge very slowly [57]. For

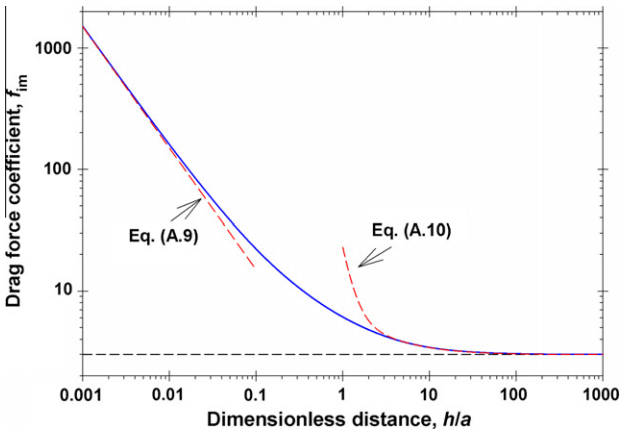

Fig. 3. Plot of the drag force coefficient for two solid particles, f_{im}, versus the distance between them, h/a, calculated by means of Eq. (A.8). At long interparticle distances we illustrate the validity of Eq. (A.10). For small values of h/a the prediction of Taylor's formula, Eq. (A.9), is drawn.

example, at $h = 2a$ one calculates 5.684 from Eq. (A.10), while the exact expression, Eq. (A.8), gives 4.790. The predictions of Eq. (A.10) are shown in Fig. 3. The series in the right-hand side of Eq. (A.8) can be summed up numerically with a high precision. For faster computations, one could use the interpolation formula [58]

$$f_{\rm im} \approx \left(3 + \frac{3a}{2h}\right)\left\{1 + 0.3766 \exp\left[-\frac{(\ln h - \ln a + 0.6789)^2}{6.297}\right]\right\}. \tag{3.13}$$

The relative error of Eq. (3.13) is smaller than 0.015 for all values of h/a. The respective curves calculated by means of Eqs. (A.8) and (3.13) coincide in Fig. 3.

In the case of *pure liquids* the jump of the tangential component of the hydrodynamic friction force across the interfaces is zero – the left-hand side of the boundary condition, Eq. (2.7), is negligible. In bipolar coordinates (Section 3.1) one simplifies Eqs. (2.4) and (2.7) to the following boundary condition:

$$\eta_{\rm d}\frac{\partial}{\partial x_1}(b\upsilon_{\rm d,2}) = \eta_{\rm f}\frac{\partial}{\partial x_1}(b\upsilon_{\rm d,2}) \text{ at } x_1 = \varepsilon. \tag{3.14}$$

We substitute Eqs. (3.6), (A.1), and (A.2) into Eq. (3.14) and transform the obtained result in series with respect to the functions $b^{3/2}V_n$ ($n = 1, 2, \ldots$). All coefficients of the derived series must be zero in order to fulfill the boundary condition. From the exact expressions for the coefficients one obtains (see Appendix B)

$$u_n = \frac{\cosh(\lambda_n\varepsilon)\sinh\varepsilon}{\cosh(2\lambda_n\varepsilon) - \cosh(2\varepsilon) + N_{\rm vr}\Delta_n}\cosh\left(\frac{\varepsilon}{2}\right) \quad (n = 1, 2, \ldots), \tag{3.15}$$

where the ratio between the viscosity of the droplet phase, $\eta_{\rm d}$, and that of the film phase, $\eta_{\rm f}$, defines the dimensionless number

$$N_{\rm vr} \equiv \frac{\eta_{\rm d}}{\eta_{\rm f}}. \tag{3.16}$$

Eq. (A.11) describes the series for the drag force coefficient, f_0, in the case of pure liquids [57] and Eq. (A.12) represents the asymptotic formula for f_0 valid at large distances between droplets. For $a/h \to 0$ the value of $f_0 \to (3N_{\rm vr} + 2)/(N_{\rm vr} + 1)$, which corresponds to the Hadamard–Rybczynski formula for the drag force coefficient of an individual droplet in the case of pure liquids.

In the case of *two bubbles* $\eta_{\rm d} \ll \eta_{\rm f}$ and we can formally substitute $N_{\rm vr} = 0$ in Eqs. (A.11) and (A.12). The applicability of serial expansion (A.12) is illustrated in Fig. 4. Eq. (A.13) corresponds to the asymptotic expression for f_0 valid for small distances between bubbles. The comparison between Eqs. (A.9) and (A.13) shows that the drag force coefficient of solid spheres increases much faster than that of bubbles with the same size. For thin films, $h \ll a$, the difference increases considerably. For example, at $h/a = 0.001$ one obtains $f_{\rm im} = 1513.4$, while for bubbles we have $f_0 = 9.4502$.

Eqs. (A.14) and (A.15) represent the asymptotic expressions for f_0 valid for small distances, $h \ll a$. Eq. (A.14) is applicable for typical viscosity ratio numbers, those are $N_{\rm vr}$ smaller than $(a/h)^{1/2}$. The comparison between the exact formula, Eq. (A.11), and the asymptotic one, Eq. (A.14), is given in Fig. 5. It is well illustrated that with the increase of the viscosity of the disperse phase the asymptotic expression (A.14) becomes operative at smaller interparticle distances, h. The respective value of the drag coefficient increases considerably.

In some cases (for bitumen emulsions) the viscosity of the drop phase is very large and one can use asymptotic expression, Eq. (A.15), valid for $N_{\rm vr} \gg (a/h)^{1/2}$. In Refs. [20–23] the reader can find some other asymptotic formulae valid for arbitrary values of $N_{\rm vr}$. The results reported in Refs. [20,21] cannot be used for bubbles.

The surface-active components change the mobility of interfaces. The value of the drag force coefficient, f, for a given system

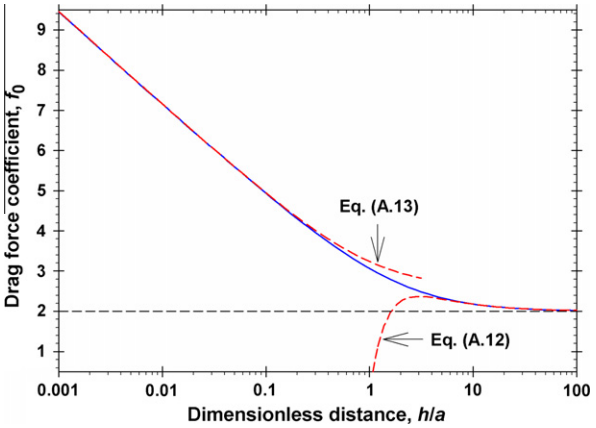

Fig. 4. Plot of the drag force coefficient for two bubbles in pure liquid, f_0, versus the distance between them, h/a, calculated by means of Eq. (A.11) with $N_{\rm vr} = 0$. The validity of approximations, Eqs. (A.12) and (A.13), is illustrated.

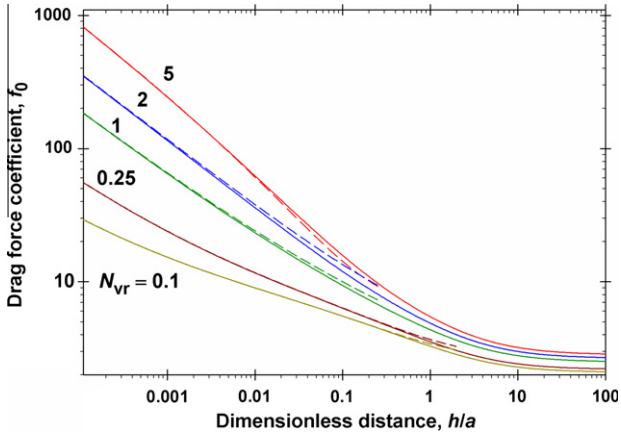

Fig. 5. Comparison between the asymptotic and exact expressions for f_0: dashed lines are calculated using Eq. (A.14); solid lines correspond to Eq. (A.11).

is always larger than that for pure liquids, f_0, and smaller than that for solid particles, $f_{\rm im}$: $f_0 < f < f_{\rm im}$. This difference is not significant for large interparticle distances when $2 < f < 3$. In contrast, the difference between f_0 and f can reach order of magnitudes for thin layers between droplets (bubbles).

4. Role of surface-active components on the interfacial mobility

4.1. General solution of the mass balance equations in the bulk

The general solution of Laplace equations, Eq. (2.10), for deviations of the bulk concentrations, $c_{\rm f,1}$ and $c_{\rm d,1}$, of the surface-active component in bipolar coordinates may be expressed in the form

$$c_{k,1} = b^{1/2}\sum_{n=0}^{\infty} C_{k,n}(x_1)P_n(\xi) \quad (k = {\rm f}, {\rm d}), \tag{4.1}$$

where the functions $C_{k,n}(x_1)$ are linear superposition of the two exponential functions, $\exp(\lambda_n x_1)$ and $\exp(-\lambda_n x_1)$. If the mathematical expression for the deviation of adsorption Γ_1 is presented in the following series with respect to the Legendre polynomials:

$$\Gamma_1 = \Gamma_0\frac{Va}{D_s}(2b)^{1/2}\frac{\sinh(\varepsilon/2)}{\cosh\varepsilon}\sum_{n=0}^{\infty} g_n P_n(\xi), \tag{4.2}$$

where the coefficients g_n ($n = 0, 1, 2, \ldots$) are unknown, then the concrete form of functions $C_{k,n}(x_1)$ can be obtained. The series in the right-hand side of Eq. (4.2) is multiplied by the Peclet number, Va/D_s, defined with respect to the surface diffusion coefficient, D_s. Therefore, the ratio Γ_1/Γ_0 is small because of the assumption for small Peclet number of the considered problem.

In the volume of the disperse phase, which contains the pole A (Fig. 2), $C_{d,n}(x_1)$ is proportional only to $\exp(-\lambda_n x_1)$. Using boundary condition (2.12) and Eqs. (4.1) and (4.2) we obtain

$$c_{d,1} = \frac{Va}{D_s}\left(\frac{\partial c_d}{\partial \ln \Gamma}\right)_0 (2b)^{1/2}\frac{\sinh(\varepsilon/2)}{\cosh\varepsilon}\sum_{n=0}^{\infty} g_n \exp[\lambda_n(\varepsilon - x_1)]P_n(\xi). \tag{4.3}$$

To obtain the solution for $c_{f,1}$ in the volume of the continuous phase together with boundary condition, Eq. (2.12), one applies the condition for symmetry with respect to the plane $x_1 = 0$, which corresponds to $z = 0$ (Fig. 1). Hence, $C_{f,n}(x_1)$ is proportional only to $\cosh(\lambda_n x_1)$ and one derives

$$c_{f,1} = \frac{Va}{D_s}\left(\frac{\partial c_f}{\partial \ln \Gamma}\right)_0 (2b)^{1/2}\frac{\sinh(\varepsilon/2)}{\cosh\varepsilon}\sum_{n=0}^{\infty} g_n \frac{\cosh(\lambda_n x_1)}{\cosh(\lambda_n \varepsilon)}P_n(\xi). \tag{4.4}$$

In general case of solutions containing one surface-active component, two sets of unknown constants have to be determined: u_1, u_2,... including in the serial expansion for the surface velocity (see Section 3.1); g_0, g_1, g_2,... appearing in the right-hand side of the expression for the deviation of adsorption, Eq. (4.2). To calculate them we will use two boundary conditions: (i) the mass balance equation for adsorption, Eq. (2.11); (ii) the continuity of the tangential stresses at the interface, Eqs. (2.3)–(2.7).

4.2. Boundary conditions for the mass balance of adsorption and for the tangential stress at the interface in bipolar coordinates

In the case of axial symmetry, the condition for the mass balance of surfactants at the interface, Eq. (2.11), in bipolar coordinates, Eq. (3.1)–(3.4), is simplified to

$$\frac{1}{\sin x_2}\frac{\partial}{\partial x_2}\left(\Gamma_0 u\frac{\sin x_2}{b} - \frac{D_s}{a}\frac{\sin x_2}{\sinh\varepsilon}\frac{\partial \Gamma_1}{\partial x_2}\right) = \frac{D_d}{b}\frac{\partial c_{d,1}}{\partial x_1} - \frac{D_f}{b}\frac{\partial c_{f,1}}{\partial x_1} \text{ at } x_1 = \varepsilon. \tag{4.5}$$

Substituting the series, Eqs. (3.10), (4.2), (4.3), and (4.4), into the boundary condition, Eq. (4.5), and taking into account that the Legendre polynomials are orthogonal, one derives an infinite set of homogeneous algebraic equations, Eq. (B.1), for the unknown coefficients (see Appendix B). The dimensionless numbers, N_{df} and N_{dd}, defined as

$$N_{dk} \equiv a\left(\frac{\partial c_k}{\partial \Gamma}\right)_0 \frac{D_k}{D_s} \quad (k = f, d), \tag{4.6}$$

characterize the ratios between the bulk diffusion fluxes and the surface diffusion flux. If the surface-active component is soluble only in the disperse phase, then $N_{df} = 0$, and vice versa, if the surfactants are soluble only in the continuous phase, then $N_{dd} = 0$. There are specific systems, for which the surfactants are soluble in both phases. For example, some alcohols are soluble in water and in oil phases and can have small adsorption at the interface (see Section 5.4). The experimental data and theoretical models show that the surface diffusion coefficient has the same order of magnitude as the bulk diffusion coefficients [44,61]. In all coefficients (see Appendix B) numbers N_{df} and N_{dd} are multiplied by $\tanh\varepsilon$. Therefore, the values of numbers $N_{df}\tanh\varepsilon$ and $N_{dd}\tanh\varepsilon$ depend mainly on the adsorption length, $(\partial\Gamma/\partial c_k)_0$, and on the combined parameter $a\tanh\varepsilon$. For large interparticle distances $a\tanh\varepsilon \to a$, while for thin layers we have $a\tanh\varepsilon \to (ah)^{1/2}$ and the relative contribution of the bulk diffusion fluxes compared to the surface diffusion decreases. The smaller bulk diffusion fluxes cannot suppress the gradients of the interfacial tension and the surfaces become more tangentially immobile.

Using Eqs. (3.1)–(3.4) we reduce the tangential stress boundary condition, Eqs. (2.3)–(2.7), in bipolar coordinates for an axisymmetric flow to the following expression

$$\frac{\partial}{\partial x_1}(b\eta_f v_{f,2} - b\eta_d v_{d,2}) = b\frac{\partial \sigma}{\partial x_2} + 2\eta_{sh}\frac{\sinh\varepsilon}{a}u + \frac{(\eta_{sh}+\eta_{dil})b}{a\sinh\varepsilon} \times \frac{\partial}{\partial x_2}\left[\frac{b^2}{\sin x_2}\frac{\partial}{\partial x_2}\left(\frac{u\sin x_2}{b}\right)\right] \text{ at } x_1 = \varepsilon. \tag{4.7}$$

In the case of diffusion-controlled processes of adsorption the two-dimensional equation of state for the interface, $\sigma = \sigma(\Gamma)$, is fulfilled at each moment of the droplets motion. Using the assumption for a small deviation of adsorption from its value at rest, Eqs. (2.13) and (2.14), we can express the Marangoni term in the right-hand side of Eq. (4.7) in the linear form

$$\frac{\partial \sigma}{\partial x_2} = \left(\frac{\partial \sigma}{\partial \Gamma}\right)_0 \frac{\partial \Gamma_1}{\partial x_2} = -\frac{E_G}{\Gamma_0}\frac{\partial \Gamma_1}{\partial x_2}. \tag{4.8}$$

Substituting the definition, Eq. (3.6), and the series, Eqs. (A.1), (3.10), (A.2), (A.4), and (4.2), into the boundary condition, Eqs. (4.7), (4.8), and taking into account that the Legendre polynomials are orthogonal, we obtain an infinite system of algebraic equations, Eq. (B.2), for the unknown coefficients (see Appendix B).

The dimensionless number N_{el} accounts for the role of Marangoni effect and N_{el} is defined as

$$N_{el} \equiv \frac{E_G a}{\eta_f D_s}. \tag{4.9}$$

This number appears in all coefficients (see Appendix B) multiplied by $\tanh\varepsilon$. The value of $N_{el}\tanh\varepsilon$ increases with: (i) the increase of the surfactant concentration because of the increase of Gibbs elasticity, E_G; (ii) the decrease of the viscosity of continuous phase, η_f, and the surface diffusivity, D_s; (iii) the increase of droplet size, a, at a fixed film thickness, h; (iv) the increase of film thickness at small interparticle distances, where $a\tanh\varepsilon \approx (ah)^{1/2}$. When the surfactant concentrations are above the CMC the Marangoni effect is negligible and one formally replaces N_{el} with zero (see Section 5.2).

Eq. (4.7) shows that the surface shear viscosity, η_{sh}, multiplies the surface velocity, u, while the surface dilatational viscosity, η_{dil}, appears as a sum with the surface shear viscosity in the tangential stress boundary condition. Moreover both contributions have different scaling rules with respect to the interparticle distance, h. The ratio between the surface-viscosity-friction forces and the bulk-viscosity-friction forces at the surface is characterized by dimensionless numbers N_{sh} and N_{dil}, defined as

$$N_{sh} \equiv \frac{\eta_{sh}}{\eta_f a} \text{ and } N_{dil} \equiv \frac{\eta_{dil}}{\eta_f a}. \tag{4.10}$$

In all coefficients (see Appendix B) these numbers appear as $N_{sh}\tanh\varepsilon$ and $(N_{dil} + N_{sh})/\tanh\varepsilon$. With the increase of these numbers the surfaces become more immobile, which takes place for smaller droplets, larger values of the surface viscosities, and smaller bulk viscosity of the continuous phase. For thin films the surface viscosity numbers have different dependences on the interparticle distance h: $N_{sh}\tanh\varepsilon \propto h^{1/2}$ and $(N_{dil} + N_{sh})/\tanh\varepsilon \propto h^{-1/2}$ [44].

In the case of large interparticle distances the expression for the drag force coefficient has a limiting value of (see Appendix B)

$$f = 3 - \left\{ 1 + \frac{\eta_d}{\eta_f} + \frac{2\eta_{dil}}{3\eta_f a} + \frac{2E_G a}{3\eta_f \left[2D_s + 2a\left(\frac{\partial c_f}{\partial \Gamma}\right)_0 D_f + a\left(\frac{\partial c_d}{\partial \Gamma}\right)_0 D_d \right]} \right\}^{-1}. \tag{4.11}$$

Eq. (4.11) gives the exact expression for the drag force coefficient of an *individual* drop (bubble), which performs a slow motion with translation velocity $V/2$. This expression could be used to determine the sedimentation velocity of diluted emulsions or diffusion coefficient of colloidal-Brownian-droplets dispersions using Stokes–Einstein approach.

5. Numerical results and discussions

5.1. Values of the dimensionless numbers

The gradient surface diffusion coefficient, D_s, and Gibbs elasticity E_G are related each others. The gradient surface diffusion coefficient is calculated from the surface chemical potential, μ_s, and the individual surface diffusion coefficient, D_{s0}, through the general relationship [61,62]:

$$D_s = \frac{D_{s0}}{k_B T}\left(\frac{\partial \mu_s}{\partial \ln \Gamma}\right)_0. \tag{5.1}$$

Using the Gibbs equation for adsorption layer, that is

$$d\sigma = -\Gamma d\mu_s, \tag{5.2}$$

and the definition of the Gibbs elasticity, Eq. (2.14), one rewrites Eq. (5.1) in the following form:

$$D_s = \frac{D_{s0} E_G}{k_B T \Gamma_0}. \tag{5.3}$$

From Eqs. (4.9) and (5.3) we obtain that

$$N_{el} = \frac{k_B T \Gamma_0 a}{D_{s0}\eta_f} = \frac{k_B T \Gamma_\infty a}{D_{s0}\eta_f}\theta \text{ and } \theta = \frac{\Gamma_0}{\Gamma_\infty}, \tag{5.4}$$

where Γ_∞ is the adsorption at close packing of the monolayer and θ is the degree of surface coverage ($0 < \theta < 1$). By analogy with the Einstein formula one defines the effective hydrodynamic radius of the adsorbed molecule in the surface layer, R_s, that is

$$R_s \equiv \frac{k_B T}{6\pi D_{s0}\eta_f}, \tag{5.5}$$

and therefore, N_{el} can be calculated from the expression

$$N_{el} = 6\pi a R_s \Gamma_\infty \theta. \tag{5.6}$$

The typical values of R_s are in the order of the radius of surfactant molecule, that of $1/\Gamma_\infty$ are in the order of πR_s^2, and radii a are larger than 1 μm, which shows that the multiplier $6\pi a R_s \Gamma_\infty$ in Eq. (5.5) is in the order of $6a/R_s$. Thus N_{el} has large values – values of $N_{el} \approx 1$ can be reached only for very small degrees of surface coverage θ.

The shear and dilatational surface viscosities depend on the degree of surface coverage. The simple linear dependence of η_{sh} and η_{dil} on θ is assumed in the literature [29], that is $\eta_{sh} = \eta_{sh0}\theta$ and $\eta_{dil} = \eta_{dil0}\theta$, where η_{sh0} and η_{dil0} are the values of the respective parameters at close packing. Thus the dimensionless numbers, N_{sh} and N_{dil}, are related to θ as follows:

$$N_{sh} = \frac{\eta_{sh0}}{\eta_f a}\theta \text{ and } N_{dil} = \frac{\eta_{dil0}}{\eta_f a}\theta, \tag{5.7}$$

see Eq. (4.10). Eqs. (5.6) and (5.7) show that: (i) with the increase of surfactant concentration, that is for larger values of θ, the dimensionless numbers, N_{el}, N_{sh}, and N_{dil}, increase; (ii) for a fixed value of θ the increase of radius a leads to the increase of the elasticity number and respectively, to the decrease of the role of surface viscosity – the numbers, N_{sh} and N_{dil}, decrease.

To obtain the formulae for number N_{dk} ($k = d, f$) we substitute the expression for D_s, Eq. (5.3), into the definition, Eq. (4.6). Using the definition of the Gibbs elasticity, Eq. (2.14), one transforms the obtained result to the following expression:

$$N_{dk} = -k_B T\left(\frac{\partial c_k}{\partial \sigma}\right)_0 a\frac{D_k}{D_{s0}}. \tag{5.8}$$

In the case of equilibrium the surface chemical potential, μ_s, is equal to the bulk chemical potentials, μ_k. The bulk phases contain small concentrations of the surface active species and the Gibbs equation, Eq. (5.2), acquires the form:

$$d\sigma = -k_B T \Gamma d\ln c_k = -k_B T\frac{\Gamma}{c_k}dc_k. \tag{5.9}$$

From Eqs. (5.8) and (5.9) we calculate that

$$N_{dk} = \frac{a c_{k,0}}{\Gamma_0}\frac{D_k}{D_{s0}} \quad (k = f, d). \tag{5.10}$$

The characteristic adsorption thickness, $\Gamma_0/c_{k,0}$, depends on the degree of surface coverage, θ, and the parameters of adsorption isotherm $c_{k,0} = c_{k,0}(\Gamma_0)$ (energy of adsorption, interaction parameter, and Γ_∞) [3,63]. Thus for a given surface active substance $\Gamma_0/c_{k,0}$ depends only on θ and it decreases with the increase of θ. For very small degrees of surface coverage the characteristic thickness has a limiting value of [3,63]

$$\frac{\Gamma_0}{c_{k,0}} \to \delta_{ads,k}\exp\left(\frac{E_{ads,k}}{k_B T}\right) \text{ for } \theta \to 0 (k = f, d), \tag{5.11}$$

where $\delta_{ads,k}$ is the thickness of adsorption layer and $E_{ads,k}$ is the energy of adsorption. Therefore, the values of N_{dk} increase with the increase of radius a and with the increase of surface coverage θ.

5.2. Concentrations above the CMC

For concentrations above the CMC the surfactant relaxation time is so small, that the interfacial tension does not change during the motion of drops and $N_{el} = 0$. The drag force coefficient, f, depends on the bulk viscosity ratio, surface viscosity, and distance between drops or bubbles. The influence of the surface viscosity on the drag coefficient, f, for bubbles and $N_{sh} = N_{dil}$ is illustrated in Fig. 6. One sees that for $N_{sh} > 10$ the interface becomes tangentially immobile and $f \approx f_{im}$. With the decrease of distance h/a the role of surface viscosity becomes more pronounced because for small values of h/a one has $(N_{dil} + N_{sh})/\tanh\varepsilon \propto (a/h)^{1/2}$ (see Section 4.2). The slope of the curves f versus h/a for small interparticle distances is the same as that for solid spheres, that is $f_{im} \propto a/h$, see Eq. (A.9), and the reader can use the asymptotic expressions reported in Ref. [38]. At large values of h/a the drag force coefficients change slightly from 2 to 3 according to the solution for an individual bubble, Eq. (4.11), and they depend on the value of the dilatational surface viscosity, that is on N_{dil}.

The solid line drawn in Fig. 6 corresponds to the hypothetical case of $N_{sh} = 20$ and $N_{dil} = 0$. One sees that the calculated drag coefficient is very close to f_0 for interparticle distances $h > a$, which is in agreement with Eq. (4.11) – the drag force of an individual drop does not depend on the surface shear viscosity. With the decrease of h/a, the values of f become closer to the calculated drag coefficient at $N_{sh} = N_{dil} = 10$, that is $N_{sh} + N_{dil} = 20$. For $h/a < 0.001$ both curves coincide. These calculations illustrate that for small distance h/a the drag force coefficient depends on the sum of surface shear and dilatational viscosities, that is on $(N_{dil} + N_{sh})/\tanh\varepsilon$.

In the case of drops the viscosity of the disperse phase influences the drag force coefficient. The calculated curves f versus

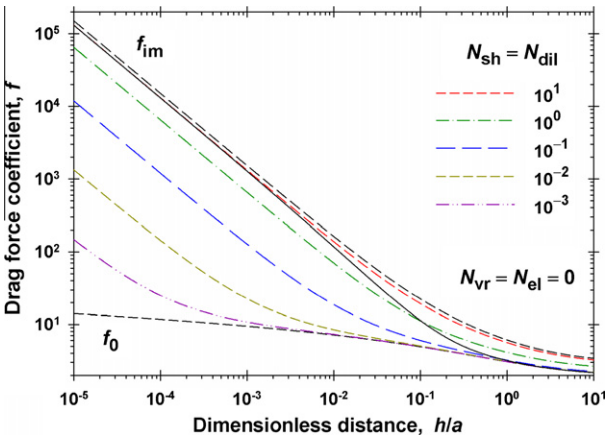

Fig. 6. Dependence of the drag force coefficient for concentrations above the CMC on the surface viscosity for $N_{vr} = N_{el} = 0$. The solid line corresponds to the hypothetical case of $N_{sh} = 20$ and $N_{dil} = 0$.

h/a for N_{vr} equals to 0.1, 1.0, and 10.0 (all other parameters are the same as in Fig. 6) are given in Supplementary material, Section S6. In all cases when $N_{vr}\tanh\varepsilon > (N_{sh} + N_{dil})$ the surface viscosity effect can be neglected, while for $N_{vr}\tanh\varepsilon < (N_{sh} + N_{dil})$ the interfacial rheology controls the mobility of surfaces. For micron-sized droplets N_{sh} is much larger than unity and the drop interfaces are tangentially immobile.

5.3. Insoluble surfactants monolayer

For an insoluble surfactants monolayer the bulk diffusion numbers, N_{dd} and N_{df}, are equal to zero and the drag force coefficient becomes a function of N_{vr}, N_{el}, N_{sh}, N_{dil}, and the distance between drops (bubbles). To illustrate the relative influence of the surface elasticity on the drag force coefficient, f, we calculate the value of f for bubbles covered by an insoluble surfactant monolayer with very low values of surface viscosity ($N_{vr} = N_{sh} = N_{dil} = 0$). Fig. 7 shows that the increase of N_{el} leads to more tangentially immobile bubble surfaces. The surface elasticity effect decreases with the decrease of the distance between bubbles – in equations N_{el} appears as $N_{el}\tanh\varepsilon$ and for small distances $N_{el}\tanh\varepsilon \approx N_{el}(h/a)^{1/2}$ (see Section 4.2). For given values of N_{el} and small distances between bubbles the drag force coefficient, f, can be orders of magnitude larger than that for a clean interface, f_0. For small interparticle distances the slopes of curves f versus h/a are parallel to that of f_0, and we found that $f \propto \ln(a/h)$, see the asymptotic expression in Ref. [38]. At large distances, h, the relative difference becomes small, in the order of 1.5, see the result for an individual bubble, Eq. (4.11).

In the case of drops the viscosity of the disperse phase influences the drag force coefficient for clean surface and the role of the surface elasticity becomes less pronounced. The curves f versus h/a for N_{vr} equals to 0.1, 1.0, and 10.0 (all other parameters are the same as in Fig. 7) are given in Supplementary material, Section S7. The following conclusions can be drawn: (i) for $N_{el} \leqslant N_{vr}$ the role of surface elasticity can be neglected; (ii) for small values of $h/a \leqslant 0.1$ and $N_{el} > 10N_{vr}$ the viscosity of drops does not influences significantly the value of f – the surface elasticity effect is predominant.

Both surface elasticity and viscosities damp the interfacial mobility in general cases. In Fig. 8 we show the role of surface coverage θ on the drag force coefficient for bubbles. The parameters correspond to low molecular weight surface active species: $\eta_f = 9 \times 10^{-4}$ Pa s; $T = 25$ °C; $D_{s0} = 3 \times 10^{-9}$ m^2/s [61]; $\eta_{sh0} = 1.45 \times 10^{-6}$ Pa m s [52]; $\eta_{dil0} = 1.0 \times 10^{-8}$ Pa m s [52]; $\Gamma_\infty = 5.58 \times 10^{-6}$ mol/m^2 [64–66]; $a = 0.3$ mm. In this case the respective dimensionless parameters are $N_{el} = 1.54 \times 10^6\theta$, $N_{sh} = 5.19\theta$, $N_{dil} = 0.037\theta$, and $N_{vr} = 0$, see Eqs. (5.4) and (5.7). One sees that for large values of surface coverage, $\theta = 0.7$, the interface is tangentially immobile for all values of h. With a 10 times decrease of surface coverage the surface becomes slightly mobile for $h/a < 3 \times 10^{-4}$, while for larger distances the surface is immobile. Even at trace amount of surface coverage, $\theta = 7 \times 10^{-5}$, the drag force coefficient is much larger than that for clean surface, f_0, and for large distances f is very close to f_{im}. This conclusion is valid also for: (i) larger bubble sizes, because in this case N_{el} increases and N_{sh} decreases; (ii) smaller bubble sizes, because in this case N_{el} decreases but N_{sh} increases.

In the case of drops the curves f versus h/a for N_{vr} equals 0.1, 1.0, and 10.0 (all other parameters are the same as in Fig. 8) are plotted in Supplementary material, Section S8. It is well illustrated that for $N_{vr} < 2$ the viscosity of the drop phase does not influence considerably the calculated value of f. At large drop viscosity, $N_{vr} = 10$, the drag force coefficients are larger for $\theta = 7 \times 10^{-5}$ and $\theta = 7 \times 10^{-4}$, but for larger degrees of surface coverage the drop viscosity does not play a role.

5.4. Soluble surfactants. Role of bulk diffusivities

In the case of soluble surfactants the bulk diffusion supplies the interface with surfactants and suppresses the interfacial tension gradients. Thus, the bulk diffusion decreases the role of Marangoni effect and fluidizes the interface. To illustrate the effect of the bulk

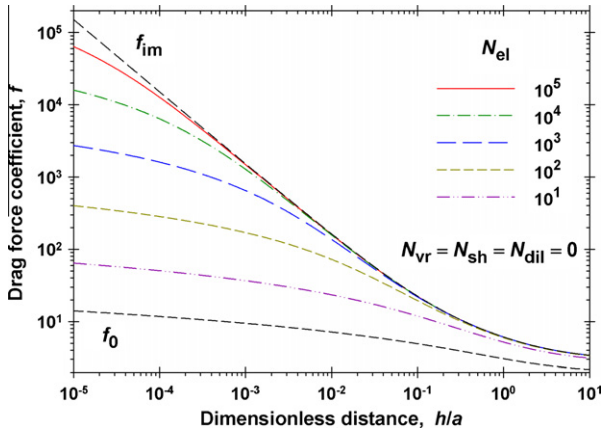

Fig. 7. Dependence of the drag force coefficient for an insoluble monolayer on the surface elasticity for $N_{vr} = N_{sh} = N_{dil} = 0$.

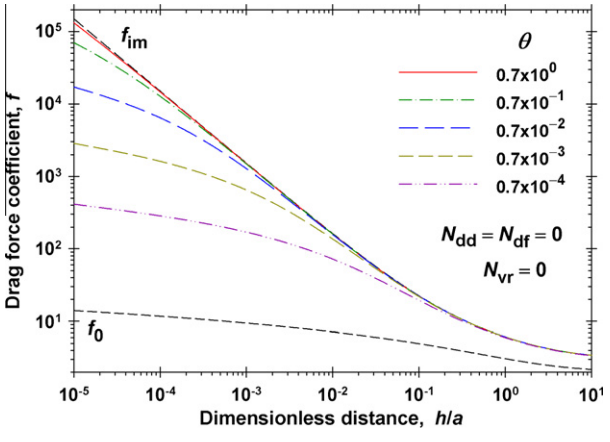

Fig. 8. Dependence of the drag force coefficient for an insoluble monolayer on the degree of surface coverage, θ, for $N_{vr} = 0$. The values of dimensionless numbers N_{el}, N_{sh}, and N_{dil}, are given in the text.

diffusion we calculate the ratio, R_f, of the drag force coefficient to the respective hypothetical drag force coefficient at zero values of N_{df} and N_{dd}, i.e. without taken into account the bulk diffusion.

First, we note that coefficients u_n ($n = 1, 2, \ldots$) explicitly depend on N_{el} and on the ratio N_{dk}/N_{el}, but not on the values of N_{dk} themselves, see Eq. (4.11) and Appendix B. From Eqs. (5.4) and (5.10) we obtain the following relationship:

$$\frac{N_{dk}}{N_{el}} = \frac{\eta_f D_k}{k_B T \Gamma_\infty^2} \frac{c_{k,0}}{\theta^2} \quad (k = f, d). \tag{5.12}$$

It is important to note that N_{dk}/N_{el} does not depend on radius a. In the simplest case of Langmuir adsorption isotherm [3,63] one has

$$K_k c_{k,0} = \frac{\theta}{1-\theta} \quad (k = f, d), \tag{5.13}$$

where K_k is the adsorption constant and Eq. (5.12) acquires the form:

$$\frac{N_{dk}}{N_{el}} = \frac{\eta_f D_k}{k_B T \Gamma_\infty^2 K_k} \frac{1}{\theta(1-\theta)} \quad (k = f, d). \tag{5.14}$$

Therefore, the role of bulk diffusion is not a monotonic function of concentrations (adsorption). The expression in the right-hand side of Eq. (5.14) has a minimum at $\theta = 0.5$ – the bulk diffusion effect is more pronounced for small and large values of surface coverage θ and less pronounced in the middle region. This conclusion is not general – for more complex isotherms the minimum of ratio N_{dk}/N_{el} appears at a value of the surface coverage different than 0.5 (see Supplementary material, Sections S4 and S5).

Second, Eq. (5.12) shows that the role of bulk diffusivity is more pronounced for surfactants with large values of the CMC, those are ionic surfactants [63–68]. The nonionic surfactants have low values of the CMC and larger adsorption for smaller bulk concentrations [63,69]. For nonionic surfactants the interfaces are immobile for very low concentrations – this conclusion is confirmed by experiments [70].

The solubility of surfactants in the disperse phase or in the continuous phase plays a different role on the suppression of the surface elasticity effect. Generally, if the surfactants are soluble in the continuous phase (oil drops in water surfactant solution) they decrease R_f smaller than that for the same inverted system (water surfactant solution drops in oil).

5.4.1. Surfactants soluble only in the continuous phase

Fig. 9 illustrates the dependence of the ratio between drag force coefficients for bubbles in nitrobenzene stabilized by different concentrations of dodecanol: 11 mM; 44 mM; and 178 mM. The parameters of the adsorption isotherm and all values of physicochemical parameters are known from the literature [61] and summarized in Supplementary material, Sections S1–S3. The bubble radius is $a = 1$ mm. One sees that for dodecanol concentration 44 mM when $\theta = 0.474$ the role of bulk diffusion is the lowest comparable to concentrations 11 mM and 178 mM, where $\theta = 0.184$ and $\theta = 0.785$, respectively. The ratio, R_f, is not a monotonic function on distance h/a – the curve R_f versus h/a has a minimum at relatively thin films (Fig. 9). This minimum is not so pronounced when the surfactant is soluble in the disperse phase (see below).

For typical water or oil soluble surfactants the value of N_{df}/N_{el} is very small – in order to have $N_{df}/N_{el} < 0.1$ the surface coverage has to be extremely low, see Eq. (5.14). Therefore, when the surfactants are soluble only in the continuous phase the bulk diffusion plays a minor role on the drag force coefficient and the system behaves as the corresponding one with the same adsorption and insoluble monolayers. To illustrate this conclusion we calculate R_f for bubbles stabilized by sodium alkyl sulfates (C_nSO_4Na) water solutions

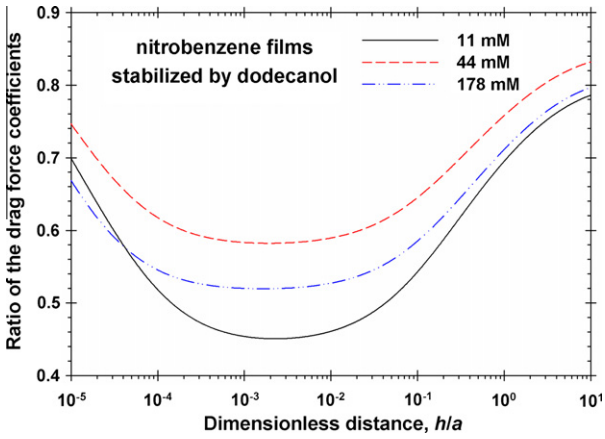

Fig. 9. Ratio of the drag force coefficients for nitrobenzene films stabilized by dodecanol at concentrations 11 mM, 44 mM, and 178 mM.

at a low degree of surface coverage, $\theta = 0.001$, (Fig. 10). The bubble radius is $a = 1$ mm and the parameters of the surface tension isotherms are given in Supplementary material, Sections S1, S2, and S4 [63]. One sees that the increase of number of carbon atoms n in C_nSO_4Na decreases the role of bulk diffusion and for $n > 10$ there is no difference between drag force coefficients calculated with and without taken into account the bulk diffusion, $R_f \approx 1$. All sodium alkyl sulfates have close values of Γ_∞ but rather different energies of adsorption. K_f increases with the increase of n and respectively for a fixed degree of surface coverage N_{df}/N_{el} decreases (see Supplementary material, Section S4). The shapes of the curves R_f versus h/a is similar to those depicted in Fig. 9. The minimum of R_f is observed for C_7SO_4Na and it is equal to 0.472.

The numerical results for the same systems and larger adsorption, $\theta = 0.01$, are given in Supplementary material, Section S9. The dependencies R_f versus h/a are analogous to those in Fig. 10 but the minimum of R_f for C_7SO_4Na is equal to 0.891. The further increase of the degree of surface coverage leads to $R_f \approx 1$ for all investigated sodium alkyl sulfates. Our calculations for oil drops (N_{vr} 0) instead of bubbles ($N_{vr} = 0$) show that for the same values of other parameters the values of R_f become closer to unity. Therefore, for most typical surfactants soluble in the continuous phase the bulk diffusion can play a minor role for very low adsorptions (concentrations).

5.4.2. Surfactants soluble only in the disperse phase

In this case $N_{df} = 0$ and the bulk diffusion of surfactants from the drop phase to the interface influences the hydrodynamic force

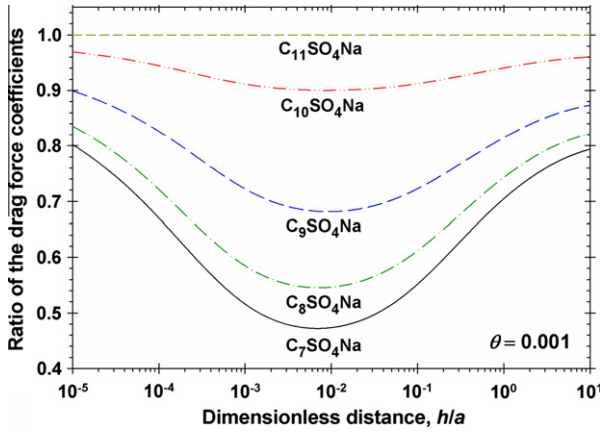

Fig. 10. Ratio of the drag force coefficients for bubbles stabilized by sodium alkyl sulfates (C_nSO_4Na) water solutions at a low degree of surface coverage, $\theta = 0.001$.

between bubbles. For small interparticle distances the diffusion from the bulk phase is more efficient than that from the narrow gap between particles (for the same inverted system) and the calculated values of f are lower. Fig. 11 shows the dependence of R_f on h/a for water drops stabilized by sodium alkyl sulfates (C_nSO_4Na) in hexadecane at a low degree of surface coverage, $\theta = 0.01$. The parameters of the interfacial tension isotherms are given in Supplementary material, Section S5, the drop radius is 1 mm and the viscosity of hexadecane is $\eta_f = 3.0 \times 10^{-3}$ Pa s. For the inverted systems hexadecane drops in the same water solutions the values of R_f are close to unity, that is the role of bulk diffusion from the disperse phase is negligible. In contrast, the drag force ratio depicted in Fig. 11 decreases with distance h and increases with the increase of the number of carbon atoms n. The minimum value of R_f is achieved for C_7SO_4Na and it is equal to 0.218. With the increase of the energy of adsorption of the respective surfactant at one and the same degree of surface coverage the bulk diffusion effect becomes lower.

For the inverted system (see Fig. 10 and Supplementary material, Section S9) we found that the increase of the degree of surface coverage ($\theta > 0.01$) eliminates the bulk diffusion effect. In the case of surfactants soluble in the drops the bulk diffusion plays a role for all concentrations. For example, for concentrations close to the CMC the degree of surface coverage is around 0.7 and the calculated values of R_f versus h/a are illustrated in Fig. 12. One sees that R_f is smaller than unity and follows the same trend as in Fig. 11. The minimum value of R_f is achieved for C_7SO_4Na and it is equal to 0.297. Even for $C_{12}SO_4Na$ the value of R_f for the smallest distance is equal to 0.841. Note, that the values of the drag force coefficients increase with the increase of surfactant concentrations because of the increase of surface elasticity and viscosity numbers (N_{el}, N_{sh}, N_{dil}). Figs. 9–12 illustrate the relative role of the bulk diffusion and give deeper understanding of the mechanism of surfactant influence.

5.4.3. Comparison between systems

In typical emulsion systems the surface active species are more soluble in one phase and less soluble or insoluble in another phase. During the homogenization process both types of emulsions are formed: the continuous phase contains surfactants and the drops are formed from another pure liquid (system I); drop phase contains surfactants at the same concentration, which are dispersed in the pure liquid (inverted system II). If the rate constants of flocculation of drops in system I are smaller than the rate constants of flocculation of the same size drops in system II, then emulsion I will survive under dynamic conditions [4,5]. The rate constants

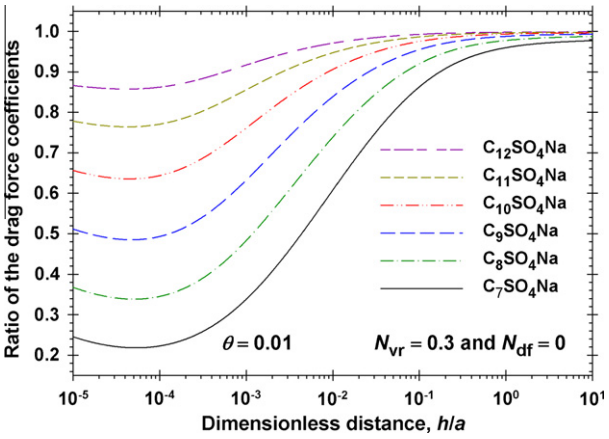

Fig. 11. Ratio of the drag force coefficients for water drops stabilized by sodium alkyl sulfates (C_nSO_4Na) in hexadecane at a low degree of surface coverage, $\theta = 0.01$.

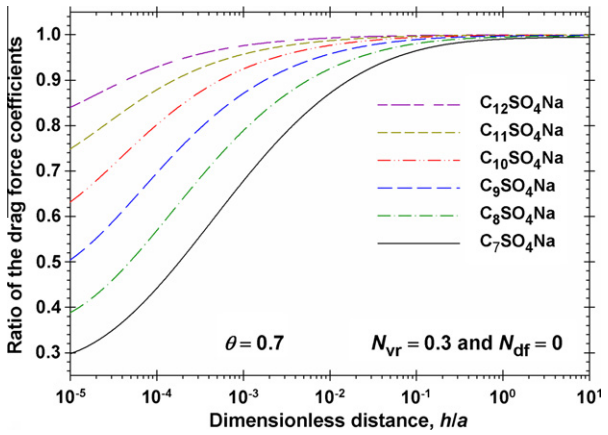

Fig. 12. Ratio of the drag force coefficients for water drops stabilized by sodium alkyl sulfates (C_nSO_4Na) in hexadecane at concentrations close to the CMC ($\theta = 0.7$).

of flocculation is integral, in which the hydrodynamic resistance is in denominator, see Eqs. (1.1) and (1.2). Thus to compare system I and system II it is important to study the ratio between the hydrodynamic resistances of these systems, β_{II}/β_I.

Figs. 11 and 12 represent R_f as a function of h/a for system parameters at which the diffusion in continuous phase does not affect the hydrodynamic resistance. Therefore, for that system β_{II}/β_I is equal to $3.3R_f$ because the viscosity of hexadecane is 3.0×10^{-3} Pa s. The larger viscosity of hexadecane comparable to that of surfactant solution leads to larger values of β_{II}. In contrast, the more efficient bulk diffusion in system II decreases hydrodynamic resistance β_{II} compared to β_I. As a result the two systems cannot be distinguished significantly from the hydrodynamic viewpoint. Note, that when the ionic surfactants are dissolved in the continuous water phase, the electrostatic interaction between drop surfaces appears and the repulsive electrostatic disjoining pressure stabilizes such emulsions [1,27,28].

If the bulk viscosity of the phase containing surfactants is larger than that of another pure liquid, then the both bulk diffusion and viscosity favor the stability of system I. Fig. 13 illustrates the dependence of β_{II}/β_I on h/a for nitrobenzene + dodecanol and water phases at three concentrations of dodecanol. The system parameters are reported in Supplementary material, Section S3. One sees that β_{II}/β_I is smaller than unity and the ratio decreases with the decrease of the gap widths. For larger concentrations of dodecanol

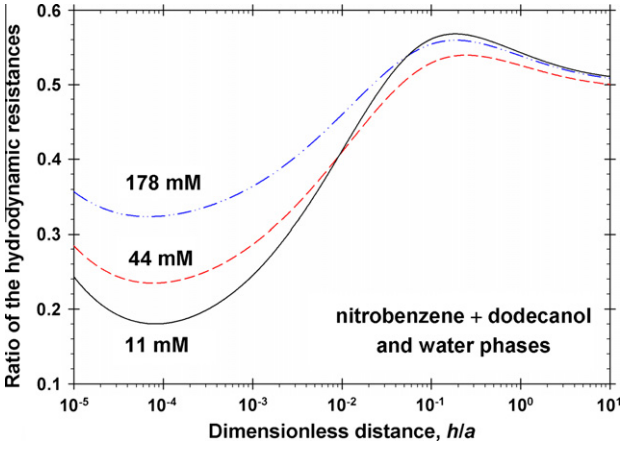

Fig. 13. Ratio between the hydrodynamic resistances β_{II}/β_I versus interparticle distance h for nitrobenzene + dodecanol and water phases. The concentrations of dodecanol are 11 mM, 44 mM, and 178 mM.

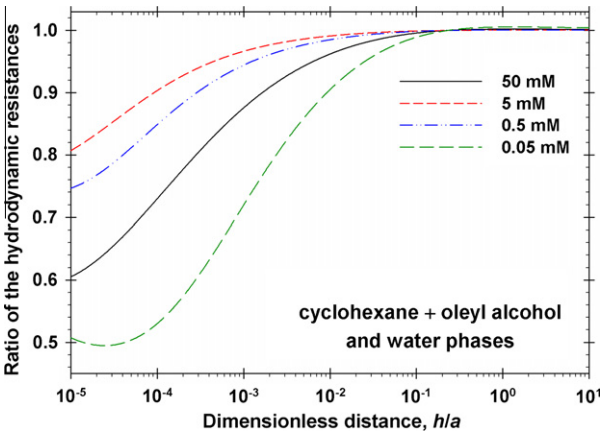

Fig. 14. Ratio between the hydrodynamic resistances β_{II}/β_I versus interparticle distance h for cyclohexane + oleyl alcohol and water phases. The concentrations of oleyl alcohol are varied from 0.05 mM to 50 mM.

the difference between the rates of flocculation of systems I and II becomes smaller.

There are systems with equal bulk viscosities – for example the bulk viscosities of water and cyclohexane at 25 °C are identical. If one uses water soluble surfactants the emulsion oil in water will be stable. In practice it is important to produce inverse water in oil emulsions stabilized by alcohols [71,72]. Fig. 14 shows an example of system formed from cyclohexane + oleyl alcohol and water phases. The parameters of the interfacial tension isotherms are reported in Supplementary material, Section S3, calculated using the experimental data from Ref. [73]. The role of oleyl alcohol concentration is well pronounced (Fig. 14) – the maximum of β_{II}/β_I is observed at a middle concentration of 5 mM. The increase of amount of oleyl alcohol to 50 mM and the decrease of concentration below 5 mM, respectively, lead to smaller values of β_{II}/β_I. Thus, in this case water in oil emulsion will survive under dynamic conditions.

6. Summary and conclusions

The stability of foams and emulsions under dynamic conditions depends on the rates of flocculation of pairs of bubbles and drops, Eq. (1.1). The higher hydrodynamic resistance between mutually approaching colloidal particles decreases the rates of flocculation and the respective dispersion is more stable. The linear hydrodynamic problem for mutual approach of two spherical drops (small Reynolds and Peclet numbers) is solved in bispherical coordinates. The continuous and disperse phases contain surfactants adsorbing at the interface. The Marangoni effect accounting for the non-uniform distribution of adsorption, the surface diffusion tending to recover the equilibrium adsorption, and the interfacial shear and dilatational viscosities are accounted for in the model (Section 2). The exact solution is obtained in terms of series with respect to the Legendre polynomials with coefficients obeying a nine diagonal linear system of equations, which is solved numerically (Section 4).

The drag force coefficient for solid particles and that for pure liquids are described by known explicit series, Eqs. (A.8) and (A.11), and useful asymptotic expressions valid for small gap widths are reported (Section 3). The role of surfactants is to modify the interfacial mobility and to increase the drag force coefficient. The effect of surface viscosity and elasticity to suppress the surface mobility in a wide range of the respective dimensionless numbers is illustrated in Figs. 6–8 for insoluble surfactant monolayers and concentrations above the CMC. For soluble surfactant the bulk diffusion from the continuous phase can decrease the drag force coefficients at small interparticle distances only for very low values of the degree of surface coverage or for surfactants with a large value of the CMC, Figs. 9 and 10. In contrast, the bulk diffusion from the disperse phase affects the hydrodynamic resistance for all degrees of surface coverage, Figs. 11 and 12, if only N_{sh} is not greater than unity. For micron-sized drops the interfacial viscosity effect is so large that the droplet interfaces are tangentially immobile for all gap widths. The obtained results can be used for comparison of the behavior of oil in water or the inverse, water in oil, emulsions in dynamic conditions, Figs. 13 and 14.

The general conclusions are: (i) the differences between the hydrodynamic resistances for both types of possible emulsions are several times (not orders of magnitude) and the role of the disjoining pressure is of a major importance for the final state; (ii) the values of the hydrodynamic resistances themselves, which are controlled on the material properties of the interfaces, are important for prediction of the rate of flocculation.

In the present work the colloidal particles are assumed to be of equal sizes. The exact solution of the problem for two drops with different radii can be solved using an analogous approach and it is an aim for our future publication.

Appendix A. Expressions for the stream functions and drag force coefficient

Using the general solution (3.8) one obtains the solution for the stream function, ψ_d, in the form [18,57]:

$$\psi_d = \frac{Va^2}{(2b)^{3/2}} \sinh\varepsilon \sinh\left(\frac{\varepsilon}{2}\right) \sum_{n=1}^{\infty} n(n+1) \frac{u_n}{\lambda_n} \{\exp[\lambda_{n+1}(\varepsilon - x_1)] - \exp[\lambda_{n-1}(\varepsilon - x_1)]\} V_n. \tag{A.1}$$

Because of the linearity of the considered problem the stream function describing the flow in the continuous phase, ψ_f, can be presented as a sum of the stream function, $\psi_{f,im}$, which gives the solution of the problem for tangentially immobile surface, and the contribution corresponding to the interfacial mobility [57]:

$$\psi_f = \psi_{f,im} + \frac{Va^2}{(2b)^{3/2}} \sinh\varepsilon \sinh\left(\frac{\varepsilon}{2}\right) \sum_{n=1}^{\infty} n(n+1) \frac{2u_n}{\lambda_n \Delta_n} \times [\sinh(\lambda_{n+1}\varepsilon) \sinh(\lambda_{n-1}x_1) - \sinh(\lambda_{n-1}\varepsilon) \times \sinh(\lambda_{n+1}x_1)] V_n, \tag{A.2}$$

where the coefficients Δ_n are defined as

$$\Delta_n \equiv \sinh(2\lambda_n\varepsilon) - \lambda_n \sinh(2\varepsilon) (n = 1, 2, \ldots). \tag{A.3}$$

Substituting Eq. (A.2) into Eq. (3.6) we derive the expressions for the velocity components. One checks directly that the obtained series obey the boundary conditions at the plane of symmetry, Eq. (3.5), and at the drop surface, Eq. (3.10). The Stimson and Jeffery solution for $\psi_{f,im}$ is well known in the literature [13,57] and

$$\psi_{f,im} = \frac{Va^2}{(2b)^{3/2}} \sinh^2\varepsilon \sum_{n=1}^{\infty} [\alpha_n \cosh(\lambda_{n-1}x_1) + \beta_n \cosh(\lambda_{n+1}x_1) + \gamma_n \sinh(\lambda_{n-1}x_1) + \delta_n \sinh(\lambda_{n+1}x_1)] V_n, \tag{A.4}$$

where the coefficients of the series, Eq. (A.4), are given by the expressions

$$\alpha_n = \frac{n(n+1)}{(2n-1)(2n+1)}, \quad \beta_n = -\frac{n(n+1)}{(2n+1)(2n+3)}, \tag{A.5}$$

$$\gamma_n = -\frac{\alpha_n}{\Delta_n}[\cosh(2\lambda_n\varepsilon) + \lambda_n \cosh(2\varepsilon)] - \frac{\lambda_{n+1}\beta_n}{\Delta_n}, \tag{A.6}$$

$$\delta_n = \frac{\lambda_{n-1}\alpha_n}{\Delta_n} - \frac{\beta_n}{\Delta_n}[\cosh(2\lambda_n\varepsilon) - \lambda_n\cosh(2\varepsilon)]. \tag{A.7}$$

Stimson and Jeffery's formula [13,57] for drag force coefficient $f_{\rm im}$ reads

$$f_{\rm im} = \sinh\varepsilon\sum_{n=1}^{\infty} \times \frac{n(n+1)}{\Delta_n}\left[\frac{\lambda_n\exp(2\varepsilon)}{2\lambda_{n-1}} + \frac{\lambda_n\exp(-2\varepsilon)}{2\lambda_{n+1}} - 1 + \frac{\exp(-2\lambda_n\varepsilon)}{\lambda_{n-1}\lambda_{n+1}}\right]. \tag{A.8}$$

Eq. (A.8) has the following asymptotic form for small interparticle distances:

$$f_{\rm im} \approx \frac{3a}{2h} \text{ at } h \leqslant a, \tag{A.9}$$

known as Taylor's formula.

Expanding Eq. (A.8) in series with respect to a/h we calculate the formula for the drag force coefficient valid at large interparticle distances

$$f_{\rm im} \approx 3 + 9\left(\frac{a}{2h}\right) - 9\left(\frac{a}{2h}\right)^2 - 15\left(\frac{a}{2h}\right)^3 + 315\left(\frac{a}{2h}\right)^4 + \ldots \text{ at } a \leqslant h. \tag{A.10}$$

Substituting solution Eq. (3.15) into Eq. (3.12) one obtains the series for the drag force coefficient, f_0, in the case of *pure liquids* [57]:

$$f_0 = f_{\rm im} - 4\sinh^3\varepsilon\sum_{n=1}^{\infty}\frac{n(n+1)}{\Delta_n} \times \frac{\cosh^2(\lambda_n\varepsilon)}{\cosh(2\lambda_n\varepsilon) - \cosh(2\varepsilon) + N_{\rm vr}\Delta_n}. \tag{A.11}$$

Expanding Eq. (A.11) in series with respect to a/h we calculate the asymptotic formula for f_0 valid at large distances between droplets

$$f_0 = \frac{3N_{\rm vr}+2}{N_{\rm vr}+1}\left[1 + \frac{3N_{\rm vr}+2}{N_{\rm vr}+1}\left(\frac{a}{2h}\right) - \frac{(N_{\rm vr}+2)(3N_{\rm vr}+2)}{(N_{\rm vr}+1)^2}\left(\frac{a}{2h}\right)^2 - \frac{5N_{\rm vr}^3 + 2N_{\rm vr}^2 - 12N_{\rm vr} - 8}{(N_{\rm vr}+1)^3}\left(\frac{a}{2h}\right)^3 + \frac{N_{\rm vr}(5N_{\rm vr}+4)(21N_{\rm vr}^2+48N_{\rm vr}+28)}{(N_{\rm vr}+1)^4}\left(\frac{a}{2h}\right)^4 + \ldots\right]. \tag{A.12}$$

Analogous to Eq. (A.10) series (A.12) converges very slowly [57].

In the case of *two bubbles* and small distances between them the following asymptotic expression for f_0:

$$f_0 \approx \ln\left(\frac{a+h}{h}\right) + 2.5407 \text{ at } h \leqslant a \text{ (for bubbles)} \tag{A.13}$$

is derived in the literature [59,60]. Ivanov et al. [22,23] arrived to similar formulae for the drag force on two bubbles approaching each other when the separation between them is very small.

In the case of *droplets* we derive the following asymptotic expressions valid for small distances $h \ll a$ and: (i) not very large droplet viscosity:

$$f_0 \approx \frac{3\pi^2 N_{\rm vr}}{16}\left(\frac{a}{h}\right)^{1/2} + \left(1 - \frac{N_{\rm vr}^2}{3}\right)\ln\left(\frac{a+h}{h}\right) + 2.5407 \text{ at } N_{\rm vr}\, h^{1/2} < a^{1/2} \tag{A.14}$$

(ii) for very large viscosity of the drop phase:

$$f_0 \approx \frac{3}{2}\frac{a}{h} - \frac{9\pi^2}{64N_{\rm vr}}\left(\frac{a}{h}\right)^{3/2} \text{ at } h \leqslant a \text{ and } N_{\rm vr}h^{1/2} \geqslant a^{1/2}. \tag{A.15}$$

The general case of asymptotic expressions, Eqs. (A.14) and (A.15), for two droplets with unequal sizes is reported in Refs. [24,25]. The calculation of close interaction between drops, with internal circulation and slip effect taken into account, is described in Ref. [26].

Appendix B. Linear system of equations for coefficients g_n and u_n

Substituting the series, Eqs. (3.10), (4.2), (4.3), and (4.4), into the boundary condition, Eq. (4.5), we derive the corresponding series with respect to the Legendre polynomials multiplied by $b^{-3/2}$. The Legendre polynomials are orthogonal and therefore, all coefficients of the series must be zero. The final form of the obtained linear system of homogeneous equations reads

$$A_{1,1}g_{n-2} + A_{1,2}g_{n-1} + A_{1,3}g_n + A_{1,4}g_{n+1} + A_{1,5}g_{n+2} + B_{1,1}u_{n-1} + B_{1,2}u_n + B_{1,3}u_{n+1} = 0 \ (n = 0, 1, 2, \ldots), \tag{B.1}$$

where in order to make the equations simpler we introduce the coefficients $g_{-2} = g_{-1} = u_{-2} = u_{-1} = u_0 = 0$. The coefficients of the linear equations, Eq. (B.1), are defined as follows:

$$A_{1,1} \equiv \frac{n(n-1)}{4(n+1)\cosh^2\varepsilon}, \quad A_{1,5} \equiv \frac{n+2}{4\cosh^2\varepsilon}, \tag{B.2}$$

$$A_{1,2} \equiv -\frac{2n^2 + n\tanh(\lambda_{n-1}\varepsilon)N_{\rm df}\tanh\varepsilon + nN_{\rm dd}\tanh\varepsilon}{2(n+1)\cosh\varepsilon}, \tag{B.3}$$

$$A_{1,3} \equiv n + \frac{n(n+1)+1}{2(n+1)\cosh^2\varepsilon} + \left[\frac{2n+1}{2(n+1)}\tanh(\lambda_n\varepsilon) + \frac{\tanh\varepsilon}{2(n+1)}\right]N_{\rm df}\tanh\varepsilon + \left[\frac{2n+1}{2(n+1)} - \frac{\tanh\varepsilon}{2(n+1)}\right]N_{\rm dd}\tanh\varepsilon, \tag{B.4}$$

$$A_{1,4} \equiv -\frac{2(n+1) + \tanh(\lambda_{n+1}\varepsilon)N_{\rm df}\tanh\varepsilon + N_{\rm dd}\tanh\varepsilon}{2\cosh\varepsilon}, \tag{B.5}$$

$$B_{1,1} \equiv \frac{n(n-1)}{2(n+1)\cosh\varepsilon}, \quad B_{1,2} \equiv -n, \quad B_{1,3} \equiv \frac{n+2}{2\cosh\varepsilon}. \tag{B.6}$$

To obtain the other set of linear equations we substitute the definition, Eq. (3.6), and the series, Eqs. (A.1), (3.10), (A.2), (A.4), (4.2), and (4.8), into the boundary condition, Eq. (4.7). The obtained result is presented as a series with respect to the polynomials V_n multiplied by $b^{3/2}$. All coefficients of the series must be zero, which leads to the following linear system of equations

$$B_{2,1}u_{n-2} + B_{2,2}u_{n-1} + B_{2,3}u_n + B_{2,4}u_{n+1} + B_{2,5}u_{n+2} + A_{2,1}g_{n-1} + A_{2,2}g_n + A_{2,3}g_{n+1} = R \ (n = 1, 2, 3, \ldots) \tag{B.7}$$

with coefficients defined by the formulae

$$B_{2,1} \equiv \frac{(n-2)(n-1)}{4(2n+1)\cosh^2\varepsilon}\frac{N_{\rm dil}+N_{\rm sh}}{\tanh\varepsilon}, \tag{B.8}$$

$$B_{2,2} \equiv -\frac{(n-1)}{(2n+1)\cosh\varepsilon}\left[N_{\rm vr} + \frac{\cosh(2\lambda_{n-1}\varepsilon) - \cosh(2\varepsilon)}{\Delta_{n-1}} + n\frac{N_{\rm dil}+N_{\rm sh}}{\tanh\varepsilon}\right], \tag{B.9}$$

$$B_{2,3} \equiv \frac{n(n+1)}{2n+1}\left(1 + \frac{1}{2\cosh^2\varepsilon}\right)\frac{N_{\rm dil}+N_{\rm sh}}{\tanh\varepsilon} - \frac{2}{2n+1}N_{\rm sh} \times \tanh\varepsilon + N_{\rm vr} + \frac{\cosh(2\lambda_n\varepsilon) - \cosh(2\varepsilon)}{\Delta_n}, \tag{B.10}$$

$$B_{2,4} \equiv -\frac{n+2}{(2n+1)\cosh\varepsilon}\left[N_{vr}+\frac{\cosh(2\lambda_{n+1}\varepsilon)-\cosh(2\varepsilon)}{\Delta_{n+1}}+(n+1)\frac{N_{dil}+N_{sh}}{\tanh\varepsilon}\right], \tag{B.11}$$

$$B_{2,5} \equiv \frac{(n+2)(n+3)}{4(2n+1)\cosh^2\varepsilon}\frac{N_{dil}+N_{sh}}{\tanh\varepsilon}, \tag{B.12}$$

$$A_{2,2} \equiv \frac{N_{el}\tanh\varepsilon}{2n+1}, \quad A_{2,1}=A_{2,3}=-\frac{A_{2,2}}{2\cosh\varepsilon}, \tag{B.13}$$

$$R \equiv \cosh\left(\frac{\varepsilon}{2}\right)\sinh\varepsilon\left[-\frac{n-1}{(2n+1)\cosh\varepsilon}\frac{\cosh(\lambda_{n-1}\varepsilon)}{\Delta_{n-1}}+\frac{\cosh(\lambda_n\varepsilon)}{\Delta_n}-\frac{n+2}{(2n+1)\cosh\varepsilon}\frac{\cosh(\lambda_{n+1}\varepsilon)}{\Delta_{n+1}}\right]. \tag{B.14}$$

The linear system of equations, Eq. (B.7), has an exact solution given by Eq. (3.15) for pure liquids when $N_{el} = N_{dil} = N_{sh} = 0$.

In the case of large interparticle distances $\varepsilon \to \infty$. From Eqs. (B.1)–(B.14) we derive the respective solution for an individual droplet. Indeed, Eqs. (B.1)–(B.14) define the leading order terms of the solution when $n = 1$:

$$(1+N_{df}+N_{dd}/2)g_1 = u_1, \tag{B.15}$$

$$\left(1+N_{vr}+\frac{2N_{dil}}{3}\right)u_1+\frac{N_{el}g_1}{3}=\frac{1}{4}. \tag{B.16}$$

Substituting Eqs. (B.15) and (B.16) into Eq. (3.12) one obtains Eq. (4.11).

The linear system of equations, Eqs. (B.1)–(B.14), is solved numerically. To increase the accuracy of calculations we chose large number N in such a way to have $\tanh(\lambda_N\varepsilon) \approx 1$. We prove that the asymptotic solution of the system for $n \geqslant N$ can be presented as

$$u_n = U\exp(-\lambda_n\varepsilon) \text{ and } g_n = Gn\exp(-\lambda_n\varepsilon), \tag{B.17}$$

where U and G are unknown constants. Substituting Eq. (B.17) into Eqs. (B.1)–(B.14) and expanding the obtained results in series for large values of n we obtain that

$$G = \frac{2U}{(2+2N_{df}+N_{dd})\tanh\varepsilon}, \quad U = \frac{\sinh\varepsilon}{U_m}\cosh\left(\frac{\varepsilon}{2}\right), \tag{B.18}$$

where parameter U_m is defined as

$$U_m \equiv 1+N_{vr}+\frac{2N_{el}}{3(2+2N_{df}+N_{dd})}+\frac{2}{3}N_{dil}. \tag{B.19}$$

All coefficients for $n < N$ are calculated numerically and those for $n \geqslant N$ are replaced by Eqs. (B.17)–(B.19). The respective contribution from u_N, u_{N+1},... to the drag force coefficient, Eq. (3.12), is calculated summing up the series

$$R_f(N) \equiv 8\sinh\varepsilon\sinh(\varepsilon/2)\sum_{n=N}^{\infty} n(n+1)\cosh(\lambda_n\varepsilon)\frac{u_n}{\Delta_n}, \tag{B.20}$$

which accounts for the tail contribution of the solution to the drag force coefficient. The obtained result reads

$$R_f(N) = 2N^2\exp(-2N\varepsilon)\left(\frac{\cosh\varepsilon}{N}+\sinh\varepsilon\right)\frac{\sinh\varepsilon}{U_m}. \tag{B.21}$$

From a physical viewpoint the minimum possible value of ε is 10^{-3} ($h = 10$ nm and $a = 1$ cm). In this case for $N = 25{,}000$ one derives that $[N\exp(-N\varepsilon)]^2 \approx 1.2\times10^{-13}$, which shows that the upper limit of the necessary number of coefficients is lower than 25,000. For the numerical solution of the linear system of equations, Eqs. (B.1) and (B.7), we order the parameters as follows: $x_1 = g_{-2}$; $x_2 = u_{-2}$; $x_3 = g_{-1}$; $x_4 = u_{-1}$; $x_5 = g_0$; $x_6 = u_0$; $x_7 = g_1$; $x_8 = u_1$; etc. Thus Eq. (B.1) includes four lower and four upper diagonal elements and subsequently Eq. (B.7) also includes four lower and four upper diagonal elements of the matrix of linear system. The numerical solution of the obtained nine diagonal linear system of equations is performed efficiently using the Thomas algorithm [74,75].

Appendix C. Supplementary material

Supplementary data associated with this article can be found, in the online version, at doi:10.1016/j.jcis.2011.11.031.

References

[1] B.V. Derjaguin, Theory of Stability of Colloids and Thin Films, Plenum Press, New York, 1989.
[2] W.B. Russel, D.A. Saville, W.R. Schowalter, Colloidal Dispersions, Cambridge University Press, Cambridge, 1989.
[3] P.A. Kralchevsky, K.D. Danov, N.D. Denkov, in: K.S. Birdi (Ed.), Handbook of Surface and Colloid Chemistry, CRC Press, Boca Raton, FL, 2008 (Chapter 7).
[4] I.B. Ivanov, P.A. Kralchevsky, Colloids Surf., A 128 (1997) 155–175.
[5] I.B. Ivanov, K.D. Danov, P.A. Kralchevsky, Colloids Surf., A 152 (1999) 161–182.
[6] K.D. Danov, N.D. Denkov, D.N. Petsev, I.B. Ivanov, R. Borwankar, Langmuir 9 (1993) 1731–1740.
[7] K.D. Danov, I.B. Ivanov, T.D. Gurkov, R.P. Borwankar, J. Colloid Interface Sci. 167 (1994) 8–17.
[8] G. Urbina-Villalba, Int. J. Mol. Sci. 10 (2009) 761–804.
[9] G. Urbina-Villalba, Langmuir 20 (2004) 3872–3881.
[10] N.A. Fuchs, Z. Phys. 89 (1934) 736–743.
[11] X. Zhang, R.H. Davis, J. Fluid Mech. 230 (1991) 479–504.
[12] I.A. Valioulis, E.J. List, Adv. Colloid Interface Sci. 20 (1984) 1–20.
[13] M. Stimson, G.B. Jeffery, Proc. Roy. Soc. A 111 (1926) 110–116.
[14] M.D.A. Cooley, M.E. O'Neill, Mathematika 16 (1969) 37–49.
[15] W. Hardy, I. Bircumshaw, Proc. Roy. Soc. A 108 (1925) 1–25.
[16] R.G. Horn, O.I. Vinogradova, M.E. Mackay, N. Phan-Thien, J. Chem. Phys. 112 (2000) 6424–6433.
[17] E. Wacholder, D. Weihs, Chem. Eng. Sci. 27 (1972) 1817–1828.
[18] S. Haber, G. Hetsroni, A. Solan, Int. J. Multiphase Flow 1 (1972) 57–71.
[19] S.H. Lee, L.G. Leal, J. Fluid Mech. 98 (1980) 193–224.
[20] R.H. Davis, J.A. Schonberg, J.M. Rallison, Phys. Fluids A 1 (1989) 77–81.
[21] G. Barnocky, R.H. Davis, Int. J. Multiphase Flow 15 (1989) 627–638.
[22] V.N. Beshkov, B.P. Radoev, I.B. Ivanov, Int. J. Multiphase Flow 4 (1978) 563–570.
[23] I.B. Ivanov, D.S. Dimitrov, B.P. Radoev, Colloid J. 16 (1979) 36–42 (in Russian).
[24] A.Z. Zinchenko, J. Appl. Math. Mech. 42 (1978) 1046–1051.
[25] A.Z. Zinchenko, J. Appl. Math. Mech. 44 (1980) 30–37.
[26] A.Z. Zinchenko, J. Appl. Math. Mech. 45 (1981) 564–567.
[27] B.V. Derjaguin, N.V. Churaev, V.M. Muller, Surface Forces, Plenum Press, New York, 1987.
[28] J.N. Israelachvili, Intermolecular and Surface Forces, Academic Press, London, 1992.
[29] D.A. Edwards, H. Brenner, D.T. Wasan, Interfacial Transport Processes and Rheology, Butterworth-Heinemann, Boston, 1991.
[30] A. Sanfeld, A. Steinchen, Adv. Colloid Interface Sci. 140 (2008) 1–65.
[31] I.B. Ivanov, K.D. Danov, K.P. Ananthapadmanabhan, A. Lips, Adv. Colloid Interface Sci. 114–115 (2005) 61–92.
[32] V. Cristini, J. Blawzdziewicz, M. Loewenberg, J. Fluid Mech. 366 (1998) 259–287.
[33] A.K. Chesters, I.B. Bazhlekov, J. Colloid Interface Sci. 230 (2000) 229–243.
[34] M.A. Rother, R.H. Davis, J. Colloid Interface Sci. 270 (2004) 205–220.
[35] A.Z. Zinchenko, M.A. Rother, R.H. Davis, J. Fluid Mech. 667 (2011) 369–402.
[36] M. Muradoglu, G. Tryggvason, J. Comput. Phys. 227 (2008) 2238–2262.
[37] H. Liu, Y. Zhang, J. Comput. Phys. 229 (2010) 9166–9187.
[38] D.S. Valkovska, K.D. Danov, I.B. Ivanov, Colloids Surf., A 156 (1999) 547–566.
[39] D.S. Valkovska, K.D. Danov, I.B. Ivanov, Colloids Surf., A 175 (2000) 179–192.
[40] T.T. Traykov, I.B. Ivanov, Int. J. Multiphase Flow 3 (1977) 471–483.
[41] T.T. Traykov, E.D. Manev, I.B. Ivanov, Int. J. Multiphase Flow 3 (1977) 485–494.
[42] I.B. Ivanov, T.T. Traykov, E.D. Manev, in: Proceedings of the VII International Congress on Surface Active Substances, Moscow, 1976.
[43] I.B. Ivanov, T.T. Traykov, Int. J. Multiphase Flow 2 (1976) 397–410.
[44] I.B. Ivanov, Pure Appl. Chem. 52 (1980) 1241–1262.
[45] Z. Zapryanov, A.K. Malhotra, N. Aderangi, D.T. Wasan, Int. J. Multiphase Flow 9 (1983) 105–129.
[46] R.B. Bird, W.E. Steward, E.N. Lightfoot, Transport Phenomena, Wiley, New York, 2001.
[47] M.J. Boussinesq, Ann. Chim. Phys. 29 (1913) 349–357.
[48] L.E. Scriven, Chem. Eng. Sci. 12 (1960) 98–108.
[49] J. Lucassen, M. van den Tempel, Chem. Eng. Sci. 27 (1972) 1283–1291.
[50] F.C. Goodrich, L.H. Allen, J. Colloid Interface Sci. 40 (1972) 329–336.
[51] F.C. Goodrich, L.H. Allen, A. Poskanzer, J. Colloid Interface Sci. 52 (1975) 201–212.
[52] J.T. Petkov, K.D. Danov, N.D. Denkov, R. Aust, F. Durst, Langmuir 12 (1996) 2650–2653.
[53] K.D. Danov, P.A. Kralchevsky, N.D. Denkov, K.P. Ananthapadmanabhan, A. Lips, Adv. Colloid Interface Sci. 119 (2006) 17–33.
[54] K.D. Danov, P.A. Kralchevsky, K.P. Ananthapadmanabhan, A. Lips, Colloids Surf., A 282–283 (2006) 143–161.

[55] K.D. Danov, D.S. Valkovska, P.A. Kralchevsky, J. Colloid Interface Sci. 251 (2002) 18–25.
[56] G.A. Korn, T.M. Korn, Mathematical Handbook, McGraw-Hill, New York, 1968.
[57] Z. Zapryanov, S. Tabakova, Dynamics of Bubbles, Drops and Rigid Particles, Kluwer Acad. Press, Dordrecht, 1999.
[58] M.P. Boneva, N.C. Christov, K.D. Danov, P.A. Kralchevsky, Phys. Chem. Chem. Phys. 9 (2007) 6371–6384.
[59] S. Kim, S.J. Karrila, Microhydrodynamics: Principles and Selected Applications, Butterworth, Boston, 1991.
[60] J.F. Harper, J. Fluid Mech. 351 (1997) 289–300.
[61] D.S. Valkovska, K.D. Danov, J. Colloid Interface Sci. 223 (2000) 314–316.
[62] S.D. Stoyanov, N.D. Denkov, Langmuir 17 (2001) 1150–1156.
[63] V.B. Fainerman, D. Möbius, R. Miller, Surfactants Chemistry, Interfacial Properties, Applications, Elsevier, Amsterdam, 2001.
[64] P.A. Kralchevsky, K.D. Danov, G. Broze, A. Mehreteab, Langmuir 15 (7) (1999) 2351–2365.
[65] P.A. Kralchevsky, K.D. Danov, V.L. Kolev, G. Broze, A. Mehreteab, Langmuir 19 (2003) 5004–5018.
[66] N.C. Christov, K.D. Danov, P.A. Kralchevsky, K.P. Ananthapadmanabhan, A. Lips, Langmuir 22 (2006) 7528–7542.
[67] I.B. Ivanov, K.P. Ananthapadmanabhan, A. Lips, Adv. Colloid Interface Sci. 123–126 (2006) 189–212.
[68] I.B. Ivanov, K.G. Marinova, K.D. Danov, D. Dimitrova, K.P. Ananthapadmanabhan, A. Lips, Adv. Colloid Interface Sci. 134–135 (2007) 105–124.
[69] I.B. Ivanov, K.D. Danov, D. Dimitrova, M. Boyanov, K.P. Ananthapadmanabhan, A. Lips, Colloid Surf., A 354 (2010) 118–133.
[70] X. Chen, S. Mandre, J.J. Feng, Phys. Fluids 18 (2006) 092103.
[71] M.J. Rang, C.A. Miller, J. Colloid Interface Sci. 209 (1999) 179–192.
[72] L. Wang, X. Li, G. Zhang, J. Dong, J. Eastoe, J. Colloid Interface Sci. 314 (2007) 230–235.
[73] Y. Takata, R. Murakami, J. Taura, T. Maki, K. Mitsutake, M. Suzuki, T. Takiue, M. Aratono, Langmuir 18 (2002) 7544–7548.
[74] C.A.J. Fletcher, Computational Techniques for Fluid Dynamics. 1. Fundamental and General Techniques, Springer-Verlag, New York, 1991.
[75] W.H. Press, B.P. Flannery, S.A. Teukolsky, W.T. Vetterling, Numerical Recipes in FORTRAN: The Art of Scientific Computing, Cambridge Univ. Press, New York, 1992.